Moonlighting α-PheRS connects JAK/STAT with Notch signaling for intestinal homeostasis

Manh Tin Ho[1], Jiongming Lu[2], Beat Suter[1]

Affiliations:

[1]Institute of Cell Biology, University of Bern, Baltzerstrasse 4, Bern 3012, Switzerland.

[2]Present address: Max Planck Institute for Biology of Ageing, 50931 Köln, Germany.

Corresponding author: beat.suter@izb.unibe.ch

Keywords: aminoacyl tRNA synthetase, Notch signaling, JAK/STAT signaling, stem cell, differentiation, proliferation, intestinal tumor

Author contributions: T.H., J.L. and B.S. conceived the ideas and designed the experiments. T.H. conducted most experiments and performed the analysis of the results. J.L. performed the loss-of-function experiments of PheRS and the mTOR signaling tests, the adult wing measurements and the FACS analysis, including analyzing their data. T.H., J.L. and B.S. wrote the manuscript.

Summary / Abstract

Phenylalanyl tRNA synthetase (PheRS) levels are elevated in multiple cancers and, interestingly, also in normal stem cells. Our results show that elevated levels of the *α-PheRS* subunit stimulate cell proliferation in different tissues, while its downregulation reduces organ size. Importantly, the proliferative activity of *α-PheRS* is independent of its aminoacyl tRNA synthase (aaRS) activity and does not visibly stimulate translation. Furthermore, stem cell-specific overexpression of *α-PheRS* caused over-proliferation in the intestine, a phenotype indistinguishable from the *Notch* RNAi phenotype in the same cells. Significantly, the phenotype caused by high levels of α-PheRS can be rescued by simultaneously overexpressing Notch, suggesting that *α-PheRS* induces this phenotype by downregulating *Notch*. High levels of α-PheRS in neuroblasts also cause the same phenotype as knocking down *Notch* in these cells, even though Notch signaling in this situation has an opposite function in promoting neuroblast proliferation and maintenance. α-PheRS therefore seems to act as a general regulator of Notch signaling. α-PheRS levels, in turn, are controlled by *Stat92E*, the downstream effector of the JAK/STAT signaling pathway that is needed for the differentiation of intestinal stem cells during tissue homeostasis under normal conditions. We found that *α-PheRS* is indeed epistatic to *Stat92E* in regulating Notch activity in the gut. Therefore, the α-PheRS subunit can transmit the activity status of the JAK/STAT pathway to the Notch pathway as a mechanism to coordinate stem cell proliferation with differentiation. In this process, α-PheRS levels balance between tissue development and tissue growth to regulate tissue homeostasis.

Introduction

Many cancer tissues display higher levels of Phenylalanyl-tRNA synthetase (PheRS, FARS or FRS) than their healthy counterparts according to the database "Gene Expression across Normal and Tumor tissue" (GENT; published 09 May 2011). Interestingly, a correlation between tumorigenic events and PheRS expression levels had been noted already much earlier for the development of myeloid leukemia (Sen et al., 1997). Despite this, a possible causative connection between elevated PheRS levels and tumor formation had so far not been reported and, to our knowledge, also not been studied. This might have been due to the assumption that higher PheRS levels could simply reflect the demand of tumorigenic cells for higher levels of translation, or it could have to do with the difficulty of studying the moonlighting function of a protein that is essential in every cell for basic cellular functions such as translation.

Aminoacyl-tRNA synthetases (aaRSs) are important enzymes that act by charging transfer RNAs (tRNAs) with their cognate amino acid, a key process for protein translation. This activity makes them essential for accurately translating the genetic information into a polypeptide chain (Schimmel and Soll, 1979). Besides their well-known role in translation, an increasing number of aaRSs have been found to perform additional functions in the cytoplasm, the nucleus and even outside of the cell (Guo and Schimmel, 2013; Nathanson and Deutscher, 2000; Smirnova et al., 2012) (Casas-Tinto et al., 2015; Gomard-Mennesson et al., 2007; Greenberg et al., 2008; Otani et al., 2002; Zhou et al., 2014). Moonlighting aaRSs regulate alternative splicing, RNA processing and angiogenesis (Lee et al., 2004). For example, the amino-acid binding site of LysRS has an immune response activity; or TrpRS inhibits the vascular endothelial (VE)-cadherin, which elicits an anti-angiogenesis activity (Tzima et al., 2005; Yannay-Cohen et al., 2009).

Cytoplasmic PheRS is one of the most complex members of the aaRSs family, a heterotetrameric protein consisting of 2 alpha- (α) and 2 beta (β)-subunits responsible for charging $tRNA^{Phe}$ during translation (Roy and Ibba, 2006). The α subunit includes the catalytic core of the tRNA synthetase and the β subunit has structural modules with a wide range of functions, including tRNA anticodon binding, hydrolyzing mis-activated amino acids, and editing misaminoacylated $tRNA^{Phe}$ species (Ling et al., 2007; Lu et al., 2014; Roy and Ibba, 2006). Precision of the initial charging reaction and proper editing are both important for the cell and the organism because mutations in the amino-acid recognition and editing sites of Drosophila *PheRS* cause sieving defects that lead to mis-incorporation of amino acids into proteins, ER stress, apoptosis, shortened life span, as well as neural degeneration (Lu et al., 2014).

We set out to address the question whether and how elevated levels of PheRS can contribute to tumor formation. To test for this activity, we studied the role of PheRS levels in the Drosophila model system with the goal of dissecting the molecular mechanism of such a moonlighting role of *PheRS.* We found that α-PheRS levels regulate cell proliferation, cell differentiation or both in different tissues and cell types. We now show that elevated levels of α-PheRS do not act simply allow higher levels of translation, but control signaling mechanisms that control differentiation and proliferation. Although the consequences of altered levels vary to some degree between tissues, we found that even in two tissues with the most divergent consequences, PheRS levels acted by repressing the Notch signaling pathway, suggesting that this regulative mechanism is responsible for all moonlighting activities of α-PheRS described here. α-PheRS levels, in turn, are controlled by JAK/STAT signaling in the intestinal system, placing α-PheRS at the intersection between two signaling pathways for the fine tuning of normal tissue homeostasis in the midgut. Focusing on the intestine and intestinal stem cells revealed that elevated α-PheRS levels are tumorigenic in the intestinal model. Given

the high demand for research on intestinal diseases and cancer (Markowitz and Bertagnolli, 2009) our work now opens new avenues to test ways to control tissue homeostasis and tumor formation.

Results

A non-canonical α-PheRS activity is sufficient to induce additional M-phase cells

To test whether elevated levels of PheRS can stimulate growth or proliferation when other aaRSs are not overexpressed, we overexpressed α-PheRS, β-PheRS, and both subunits together in the posterior compartment (P) of wing discs using the *engrailed-Gal4* (*en-Gal4*) driver. In this assay the anterior compartment expresses normal endogenous levels and serves as an internal control. When α-PheRS was overexpressed in the posterior compartment either alone or together with β-PheRS, the mitotic marker phospho-histone H3 (PH3) revealed a 40% increase in mitotic cells in the posterior (P) compartment relative to the anterior (A) one of the same disc (Fig 1A-C). Because elevated levels of the α-PheRS subunit alone are sufficient for the increase in mitotic cells, this effect is unlikely caused by increased $tRNA^{Phe}$ aminoacylation activity and translational activity, which requires both subunits.

To test this interpretation, we made a mutant version of α-PheRS in which Tyr412 and Phe438 are replaced by Cysteins. These substitutions are predicted to block the entrance into the phenylalanine binding pocket, preventing binding of Phe and aminoacylation of $tRNA^{Phe}$ by the mutant $PheRS^{Cys}$ (Finarov et al., 2010). To test whether the $PheRS^{Cys}$ substitution indeed reduces the aminoacylation activity of PheRS, we expressed mutant and wild-type α-PheRS subunits together with β-PheRS subunits in E. coli, purified them and performed aminoacylation assays. α-$PheRS^{Cys}$ together with wild-type β-PheRS produced the same background signal as the α-PheRS subunit alone, and this signal was clearly lower than the one obtained with wild-type α-PheRS plus β-PheRS (Supplementary Fig S1). The same mutations were also introduced into a genomic clone and the resulting transgenic *α-PheRS*^{Cys} was not

able to rescue the *α-PheRS*^{G2060} mutant, indicating that the Cys mutant is indeed not functional in aminoacylation in vivo in Drosophila. Overexpressing a transgenic *α-PheRS*^{Cys} in the posterior compartment of the wing disc also caused a 67% increase in the number of mitotic cells in the above assay (Fig 1C). The fact the mutant *α-PheRS*^{Cys} version caused an increase in mitotic cells at least as strongly as the wild-type *α-PheRS,* together with the fact that β-PheRS overexpression was not needed for this effect, clearly demonstrates that the canonical function of *PheRS* is not required to cause the elevated frequency of mitotic cells.

We also tested directly whether PheRS overexpression is unable to cause elevated translation as we expected. For this, we analyzed protein synthesis activity in the two wing compartments by puromycin staining using the ribopuromycylation method (RPM) (Deliu et al., 2017). Overexpression of the transcription factor dMyc increases protein synthesis activity and was therefore used as a positive control for detection of elevated translation and PMY labeling (Deliu et al., 2017). Indeed, when comparing signal intensity in the posterior compartment to the intensity in the anterior compartment of the same disc, dMyc overexpression significantly increased the anti-PMY signal in the expressing posterior compartment. In contrast, neither overexpression of α-PheRS alone nor combined with β-PheRS increased the puromycin labeling, a proxi for general translation, in the overexpressing compartment (Fig 1D-E'', F). The combined results therefore demonstrate unambiguously that elevated α-PheRS levels cause additional cells to be in mitosis through an aminoacylation- and translation-independent, non-canonical activity. α-PheRS levels might specifically slow down progression through M-phase, causing higher numbers of cells to remain in the PH3-positive state. Alternatively, they might either promote over-proliferation of mitotic cells or induce proliferation in non-cycling cells.

High α-PheRS tolerance in an organ with tight size control

To find out whether the increased number of mitotic cells in the region expressing higher α-PheRS levels leads to a different compartment size, we measured the size of two clearly defined regions in the posterior (P) and the anterior (A) compartment of the adult wing as shown in Fig 2A. Normalizing the size of the posterior region (P) to the size of the anterior region (A), we calculated the P/A ratio (Fig 2B). Even though α-PheRS alone was sufficient to induce additional mitotic cells in larval discs, this did not cause the formation of a larger wing in the adult. Co-overexpression of both subunits was needed to cause a small, but significant increase of the posterior region of the wing (Fig 2B). This size increase does not appear to be a general property of elevated aaRS levels because overexpression of Glycyl-tRNA synthetase (GlyRS; REF (Niehues et al., 2015)) with the same driver did not increase wing size (Fig 2B). The final size of this organ is tightly controlled by different mechanisms that are only partially understood, but are capable of compensating for differences in growth and proliferation such that the compartments reach their correct final size even if they grew at different rates at an earlier stage (Hariharan, 2015; Martin and Morata, 2006). To better understand the consequences of high PheRS levels in the discs, we studied its effect on dissociated cells and found that elevated PheRS levels primarily affected cell size whereas proliferation remained controlled or was compensated for (Supplementary data, Fig S2A,B).

We considered the possibility that PheRS might signal availability of Phe to TORC1, which links cell growth to amino acid availability (Laplante and Sabatini, 2012; Wullschleger et al., 2006). Such a mechanism would be analogous to the function of LeuRS in this pathway (Bonfils et al., 2012; Han et al., 2012). However, experimental testing of this hypothesis did not uncover any evidence for such a signaling function (Supplementary data, Fig S3A,B).

The *α-PheRS* subunit accelerates proliferation in different tissues and its knockdown reduces organ size

To test the effects of PheRS levels on proliferation directly and in other cell types, we set up a mosaic analysis with repressible cell marker (MARCM; (Wu and Luo, 2006) assay in the follicle cells. Twin spot clones were generated with one clone overexpressing PheRS and the GFP marker, and its twin clone expressing normal endogenous levels of PheRS and serving as an internal control (Fig 3A). The results of this experiment showed that clonal overexpression of both subunits of PheRS accelerated the proliferation of the overexpressing cells on average by 32% (Fig 3B). Overexpression of GFP with only the β-PheRS subunit or with GlyRS did not significantly promote clonal expansion (Fig 3B), confirming that the activity of stimulation growth and proliferation is specific for PheRS and not a general role of aaRSs. Interestingly, overexpression of GFP with the α-PheRS subunit alone also stimulated cell proliferation autonomously by 30% (Fig 3B) and, intriguingly, this was very close to the 32% increase calculated for the clone overexpressing both PheRS subunits (Fig 3B). Remarkably, the higher number of mitotic cells observed upon α-PheRS overexpression in the posterior compartment of the larval wing discs (Fig 1C) was in a comparable range as the proliferation increase in the follicle cell assay (Fig 3B). These results therefore suggest that α-PheRS levels promote cell proliferation and that it has this activity in different tissues.

Overexpression of *α-PheRS*^{Cys} alone and *α-PheRS*^{Cys} together with *β-PheRS (PheRS*^{Cys}) stimulated clonal growth and cell proliferation in the follicle cell twin spot experiment by 28% and 25%, respectively (Fig 3B), again confirming that this is an aminoacylation-independent activity. It is tempting to speculate that the slightly lower increase in proliferation upon overexpressing the mutant *α-PheRS*^{Cys} (28%) in twin spot clones compared to wild-type *α-*

PheRS (30%) could be due to reduced translation caused by the overexpression of an inactive α subunit that is predicted to partially act as a dominant negative subunit for the aminoacylation function. If this proliferation function is important for development and homeostasis, reduced *α-PheRS* activity should lead to problems in these processes. Because *α-PheRS* and *β-PheRS* are both essential genes in Drosophila (Lu et al., 2014), we used RNAi to reduce their activity in specific tissues by RNAi (Fig S4A,B). Indeed, knock down in the developing eye reduced the adult eye, whereas knockdown in the larval fat body reduced the size of the entire pupae. Furthermore, RNAi knockdown *α-PheRS* or *β-PheRS* in Kc cells caused these cells to proliferate more slowly than the control cells (Fig S4C). Although it is not clear from these results, which activity of PheRS causes this effect, the phenotypes observed are consistent with a direct function in regulating proliferation.

α-PheRS promotes stem cell proliferation in the midgut and high expression leads to hyper- and dysplasia

Tissue growth and homeostasis play important roles in developing and outgrown animals, and they require tight control of stem cell self-renewal and differentiation of daughter cells. The Drosophila midgut is a powerful model to analyze these mechanisms and their interplay. Intestinal stem cells (ISCs), also referred to as adult midgut progenitors (AMPs) in the larval gut, can either divide asymmetrically or symmetrically. After an asymmetric division, one daughter cell differentiates into an absorptive enterocyte (EC) or a secretory enteroendocrine (EE) cell, the other keeps its stem cell identity. We investigated the effect of overexpression of each PheRS subunit in larval ISCs by using the *esg-Gal4* driver, which is specifically expressed in ISCs. Co-expression of *UAS-YFP* allowed us to monitor the activity of the *esg-Gal4* driver. The results demonstrated that overexpression of Myc::α-PheRS alone in the larval midgut

caused the numbers of YFP positive ISC cell clusters in the posterior midgut to increase. In addition, the number of YFP positive cells per cluster increased as well (Fig 4A, B, D-D'). The increase of both numbers was significant when compared to posterior midguts expressing normal levels of α-PheRS (Fig 4A, B, C-C'). Overexpression of β-PheRS::V5 alone did not show such a phenotype (Fig 4A, B, E-E'). Interestingly, when both PheRS subunits were overexpressed, the guts also showed an increase in the number of YFP positive ISC clusters, however, the increase was less pronounced and the number of YFP positive cells per cluster remained unchanged (Fig 4A, B, F-F').

Driving the expression of the α-PheRS^{Cys} mutant alone in ISCs also produced additional ISCs, indicating again that the aminoacylation function is not required for this activity (Fig 4G). Surprisingly, however, this treatment induced the over-proliferative phenotype in both anterior and posterior areas of the larval midgut (outlined with white dashed lines, Fig 4G, G') while the overexpression of wild-type Myc::α-PheRS only gave rise to high numbers of ISCs in the posterior midgut (Fig 4D, D'). Interestingly, elevated α-PheRS^{Cys} levels also caused the appearance of a more severe, tumor-like phenotype, where individual ISC clusters could not be discerned anymore. Furthermore, instead of the wild-type gut phenotype, characterized by a majority of ECs with large nuclei, interspersed with occasional ISC clusters with smaller nuclei (as seen in the YFP overexpression control, Fig 4C, C'), we observed a phenotype where ECs and ISCs could not be distinguished based on the size of their nuclei, but emerged as a larger cell population with intermediate size nuclei (Fig 4G'). Many of these cells expressed the *esg*>YFP stem cell marker at high levels, but others displayed only a very weak YFP signal. One possible interpretation of this phenotype could be that α-PheRS^{Cys} overexpressing ISCs progress through the cell cycle more rapidly such that they are not able to grow to their proper size and do not have sufficient time to turn over the YFP. Staining these guts for the mitotic marker PH3 demonstrated that the posterior midgut contained clearly more

and a higher proportion of PH3 positive cells. Significantly, more cells were labelled by anti PH3 staining in the posterior midgut when α-PheRS or the α-PheRS^{Cys} mutant were overexpressed alone in ISCs (Fig 4H, I). Again, this suggests that cells in these areas display an elevated proliferation rate.

In a normal adult midgut, ISCs are found as characteristic single cells or as pairs with their daughter enteroblast (EB). Both cell types are labeled with YFP when their expression is driven by *esg*-Gal4 (Fig 4J). Overexpression of only α-PheRS or α-PheRS^{Cys} in these adult ISCs caused a strong phenotype, too. It induced hyperplasia and dysplasia in regions R4-R5 of the posterior midgut. Similar to the hyperplasia phenotype observed in the larval gut, we observed cells adjacent to ISC clusters displaying the YFP stem cell marker, even though they contained large nuclei (Fig 4J'-J"), indicative of a dysplasia phenotype. We conclude that in the larval and adult guts, elevated α-PheRS expression can elevate the proliferation rate of stem cells and lead to hyper- and dysplasia.

Elevated α-PheRS levels prevent proper differentiation and gut homeostasis by downregulating Notch signaling

Asymmetric divisions of ISCs give rise to a new ISC and an undifferentiated EB. Differential Delta/Notch signaling between the new ISC and the EB causes the latter to either differentiate into an absorptive EC or a secretory EE (Micchelli and Perrimon, 2006; Ohlstein and Spradling, 2007). To investigate how α-PheRS affects the fate decision in this lineage, we studied the cell population in the posterior midgut. In larval and adult guts, the over-proliferation phenotype caused by α-PheRS^{Cys} overexpression showed a significantly elevated ratio between EEs and ECs (Fig 5A-A', B-B', C). The overexpression of *α-PheRS* alone with the *esg-Gal4* driver caused the same changes, albeit with a slightly lower expressivity (Fig 5C). These observations

indicate that overexpression of α-PheRS or α-PheRS^{Cys} directs EB differentiation to the EE fate and interferes with EC differentiation.

Differentiating ISC daughter cells, EBs, adopt the EE fate when their *Notch* activity is low and the EC fate if their *Notch* activity is high (Takashima et al., 2011). Furthermore, because *Notch* activity is needed for EB differentiation, reduced *Notch* activity leads to EE-like and ISC-like tumors (Micchelli and Perrimon, 2006; Patel et al., 2015; Wang et al., 2015; Yin and Xi, 2018). Indeed, in regions where the normal cellular composition of the larval gut was transformed, we observed an increase in the number of cells and in particular a cell population with intermediate size nuclei upon RNAi treatment of *Notch* with the *esg-Gal4* driver (white dashed line, Fig 5D-D'). The similarity between the two phenotypes suggests that overexpression of *α-PheRS* or *α-PheRS^{Cys}* might cause this phenotype by reducing *Notch* activity. Indeed, as seen in Fig 5F, overexpression of *α-PheRS* and *α-PheRS^{Cys}* downregulates the *Notch* activity reporter NRE-EGFP (Notch response element promoter driving the expression of eGFP; (Housden et al., 2012) and overexpressing *Notch* together with *α-PheRS^{Cys}* in the same midgut ISCs rescued the tumor-like midgut phenotype, giving rise to midguts with a wild-type appearance (Fig 5A", B", E-E'). This shows that α-PheRS levels control *Notch* activity and that high α-PheRS levels cause the tumor-like phenotype in the midgut by downregulating *Notch* activity.

α-PheRS is a novel general repressor of Notch signaling

Developing larval brains contain neuroblast (NB) stem cells that divide asymmetrically to either keep the stemness and or to differentiate into neuronal cells. *Notch* signaling plays a crucial role in this process (Ables et al., 2011; Giachino and Taylor, 2014), but in contrast to the situation in the gut, loss of *Notch* prevents NB self-renewal, and ectopic expression of *Notch*

leads to tumor formation (de la Pompa et al., 1997; Grandbarbe et al., 2003; Hatakeyama et al., 2004). This opposite role of *Notch* makes the NB lineage an ideal complementary system to test whether α-PheRS is a general component of the *Notch* pathway. Driving α-PheRS or the α-PheRS^{Cys} expression in NBs with the *inscutable-Gal4 (incs-Gal4)* driver resulted in significantly smaller central brains (CB), the region where the NBs are located (Fig 6A-A'', B). In contrast, this treatment had little or no effect on the size of the optic lobes (OL). The phenotype was indistinguishable from the phenotype caused by *N* knock-down (Fig 6B), and co-overexpression of Notch with α-PheRS^{Cys} in neuroblasts rescued the brains to wild-type size (Fig 6B).

Type II neuroblasts are particularly suited to analyze effects on neuroblast differentiation. Targeting specifically the 8 type II neuroblasts in central brain lobes with *α-PheRS* or *α-PheRS*^{Cys,} overexpression, resulted in half of the central brains in a strong reduction of the number of neuroblasts, and the resulting central brain lobes ended up smaller (Fig 6C and Supplementary Fig S5). Knocking down *N* in type II NBs with RNAi and the same driver combination resulted in a similar phenotype, but with a higher expressivity. On the other hand, overexpression of N in α-PheRS overexpressing type II neuroblasts partially rescued the number of type II neuroblasts to wild-type numbers and it restored the normal size of the brain (Fig 6C and Supplementary Fig S5). Because the effect on *Notch* signaling is the same in guts and brains, two tissues where Notch has opposing functions on cellular differentiation, we conclude that *α-PheRS* is a novel general repressor of *Notch* signaling.

Transcription factor STAT92E of the JAK/STAT pathway regulates α-PheRS levels

Under normal condition, the STAT92E induces the progenitors to differentiate into ECs via regulating Notch activity (Herrera and Bach, 2019). Under stress conditions, like bacterial

infections, secreted Unpaired3 (*Upd3*), is a cytokine of the JAK/STAT signaling pathway that activates ISC proliferation and differentiation to repair damaged parts of the gut (Buchon et al., 2009; Lin et al., 2010). Upd3 not only activates JAK/STAT signaling in ISCs, but also *Notch* activity to enhance ISC proliferation and to promote EC differentiation, respectively (Jiang et al., 2009). We therefore tested whether α-PheRS could possibly coordinate JAK/STAT with Notch signaling. The *Stat92E* gene encodes the transcription factor at the downstream end of the JAK/STAT pathway. Using the hypomorphic $Stat92E^{HJ}$ allele, we tested whether suppressing JAK/STAT signaling affects α-PheRS expression. Indeed, $Stat92E^{HJ}$ mutants displayed elevated levels of α-PheRS in Delta-positive ISC cells (Fig 7A-B"). Consistent with this result, *Stat92E* knock-down by RNAi with the *esg-Gal4* driver also showed elevated α-PheRS levels in ISC cells (Fig7C-C"). As shown in Fig 7 D-D', E-E', F-F', G, the levels of α-PheRS significantly increased in ISCs/EBs. The fact that two different approaches to reduce *Stat92E* activity lead to higher α-PheRS levels in ISCs/EBs clearly demonstrates that *Stat92E* regulates α-PheRS levels in these cells.

Surprisingly, RNAi knock down of *Stat92E* with the *esg-Gal4* driver not only affected α-PheRS levels in ISCs, but also in some neighboring polyploid ECs, but not in distant ECs (arrows in Fig7C", F) (Fig7G). Because we also observed this phenotype in $Stat92E^{HJ}$ mutants (arrows in Fig 7E) (Fig 7G), this is unlikely to be an off-target effect of the RNAi. It thus appears that *Stat92E* can normally control α-PheRS levels also in a cell non-autonomous way. To test if *Stat92E* is not only required for downregulation of α-PheRS, but also sufficient, we overexpressed *Stat92E* in ISCs and EBs. Indeed, elevated–STAT92E levels reduced the α-PheRS signal in ISCs and EBs (Fig 7H-I"). On the other hand, high levels of α-PheRS did not affect *Stat92E* activity when assayed with the *10X STAT92E-GFP* reporter (Bach et al., 2007) (Fig 7J-K"'). We conclude that *Stat92E* can regulate α-PheRS levels specifically in EBs and ISCs to maintain stem cell homeostasis. To study the epistatic relationship between *Stat92E*

and *α-PheRS* and to find out whether downregulation of α-PheRS is indeed mediating the modulation of Notch by JAK/STAT, we expressed STAT92E and α-PheRS individually and together and measured the resulting Notch activity in adult guts using the NRE-EGFP reporter (Fig 7M). Whereas elevated levels of STAT92E led to elevated expression of the Notch activity reporter, co-overexpression of α-PheRS and STAT92E reverted this effect and even downregulated the Notch activity reporter NRE-EGFP further to 44% of wild-type Notch activity. This is a similar to the downregulation observed when only α-PheRS levels were elevated (41% of wild-type Notch activity). Elevated levels of STAT92E have little effect on cellular identity in the gut (Fig 7L'''). In contrast, co-overexpression of both, leads to the same tumor-like midgut phenotype (Fig 7L'') like overexpression of *α-PheRS* alone (Fig 4J', 7L'), indicating that *α-PheRS* is epistatic to *STAT92E*. Together with the results that α-PheRS regulates Notch signaling and that STAT92E downregulates α-PheRS, we therefore identified α-PheRS as an intermediate factor that links the JAK/STAT pathway to Notch signaling to regulate gut homeostasis.

Discussion

Our work revealed that *PheRS* not only charges tRNAs with their cognate amino acid Phe, but that it also performs moonlighting functions in regulating cell proliferation and differentiation in different tissues. Levels of α-PheRS are critical for these regulative processes and these levels are generally elevated in healthy stem cells compared to differentiated cells. Similarly, many tumor cells show elevated α-PheRS levels compared to their healthy counterparts and a positive correlation between these levels and tumorigenic events had been noted quite some time ago (Sen et al., 1997). Several circumstantial and direct evidence show that elevated α-PheRS levels do not simply allow higher translational activity to overcome a growth rate restriction imposed by hypothetically limiting levels of PheRS. In fact, PheRS is unlikely to be rate-limiting for cellular growth. because animals with only one copy of the *α-PheRS* or *β-PheRS* gene do not show a phenotype (Lu et al., 2014) and tissue culture cells can be stimulated to grow more rapidly without stimulating the expression of the two PheRS genes (Chen et al., 2003) (Lu et al., 2014). Indeed, directly measuring translational activity *in situ* (Fig 1D-D") showed the same levels of translation whether *α-PheRS* was overexpressed or not. Furthermore, aminoacylation of $tRNA^{Phe}$ requires the tetrameric protein $\alpha_2\beta_2$*-PheRS.* However, overexpression of an aminoacylation-dead *α-PheRS*^{Cys} mutant subunit alone, (without simultaneous overexpression of the β-PheRS subunit) already lead to the accumulation of numerous additional dividing cells, closely resembling the phenotype observed when the wild-type gene was expressed in the same way. We therefore conclude that this activity of *α-PheRS* is independent of the translational function of *PheRS.*

The notion that the α-PheRS subunit can be stable and function independently of the β-subunit was surprising because previous results showed that the two subunits were dependent on the presence of the other subunit for their stability (Antonellis et al., 2018; Lu et al., 2014).

Our results now show that this requirement does not apply to all cell types. In young follicle cells, ISCs and possibly other dividing cells, the overexpression of the α-PheRS subunit alone results in higher levels of α-PheRS accumulation and, in particular when elevated levels were induced in gut ISCs and EBs, this produced a strong phenotype. This suggests that the α- and β-PheRS subunits function together in every cell to aminoacylate $tRNA^{Phe}$, but in addition, the α-subunit can be stable in specific cell types, such as stem cells, where it assumed a novel function in regulating cell proliferation and differentiation.

PheRS is not the only aaRS family member for which roles beyond charging tRNAs have been identified (Dolde et al., 2014). For instance, MetRS/MRS is capable of stimulating the rRNA synthesis (Ko et al., 2000), GlnRS/QRS can block the kinase activity of apoptosis signal-regulating kinase 1 (ASK1) (Ko et al., 2001) and a proteolytically processed form of YARS/TyrRS acts as a cytokine (Casas-Tinto et al., 2015; Greenberg et al., 2008). aaRSs are, however, also not the only protein family which evolved to carry out more than one function. In recent years it has become increasingly evident that many if not most proteins have evolved to carry out not only one, but two or more functions, providing interesting challenges to figure out, which of their activities are important for the individual functions of a protein (Dolde et al., 2014).

We found that elevated levels of α-PheRS promote cell proliferation in different cell types. In follicle cells, more cells were produced in the α-PheRS overexpressing clones compared to wild-type clones. In wing disc, more mitotic cells were detected in the α-PheRS overexpressing compartments. These phenotypes are not only independent of the aaRS activity (Fig 1D-F), they also do not reflect a function in sensing the availability of its enzymatic substrate Phe and transmitting this information to the major growth controller, the TOR pathway, like the aaRS members TrpRS or LeuRS (Fig S3) (Adam et al., 2018; Bonfils et al.,

2012; Han et al., 2012). In the gut tissue, elevated α-PheRS$^{(Cys)}$ levels produced 2-5 times as many cells with intermediate size nuclei that stained positive for stem cell markers. Similarly, these guts also contained 5-8 times as many mitotic cells when α-PheRS$^{(Cys)}$ was overexpressed. Together, these results strongly suggest, that also in this situation the higher levels of α-PheRS induced over-proliferation of ISCs.

Overexpression of α-PheRS in the gut ISCs additionally interfered with cell fate decisions by driving ISCs to duplicate and to differentiate into EEs. The combination of these effects results in a "tumor-like" phenotype, that had been described as ISC/EE tumor phenotype that results from downregulation of *Notch* activity (Korzelius et al., 2014; Micchelli and Perrimon, 2006). Interestingly, mis-regulating proteins involved in EE fate specification, like downregulation of Tramtrack69 or upregulation of its adaptor protein Phyllopod, also results in this phenotype (Wang et al., 2015; Yin and Xi, 2018), suggesting that α-PheRS levels, through their activity on Notch signaling, induce the "tumor-like" phenotype in the gut tissue not only by increasing stem cell proliferation, but also by driving the differentiating cells into an EE fate.

The gut phenotype caused by elevated levels of α-PheRS points to the importance of controlling and fine tuning these levels. We found that the JAK/STAT pathway is able to control cellular α-PheRS levels and that it acts upstream of α-PheRS levels in controlling Notch signaling. Interestingly, under normal condition, JAK/STAT signaling, which is known to stimulate progenitor cell differentiation to regulate the normal tissue homeostasis (Herrera and Bach, 2019), downregulates *α-PheRS* levels and, consequently, activates Notch signaling and promotes differentiation of the progenitor cells into ECs. Therefore, regulation of α-PheRS levels links the two signaling pathways and implicates *PheRS* not only in the regulation of cell proliferation, but also in the regulating stem cell and tissue homeostasis by connecting the

Notch to the JAK/STAT signaling pathway. STAT92E is a transcription factor, but none of the published reports on STAT92E targets lists the *α-PheRS* gene (Bina et al., 2010; Muller et al., 2005; Wang et al., 2013). A direct repression of *α-PheRS* gene expression by STAT92E appears therefore unlikely even though it is also possible that this interaction escaped detection because it happens in too few cells of the analyzed cell types.

An interplay between the JAK/STAT and the Notch signaling pathways to maintain ISCs homeostasis has been noted before. In regenerating midguts, damaged ECs release Upd cytokines to activate JAK/STAT signaling in ISCs and to promote ISC division (Jiang et al., 2009). This also stimulates Delta/Notch activity to promote EC differentiation (Jiang et al., 2009). Knocking down *Stat92E* reduced *Delta* mRNA levels, and *Notch* target genes were downregulated when *Stat92E* activity was abolished in progenitor cells (Jiang et al., 2009). In this situation the JAK/STAT signaling therefore feeds into the downstream Notch signaling pathway. Our work now reveals an unexpected missing link between these two pathways which have drawn considerable attention for cancer research.

Relevance of moonlighting function of α-PheRS for tumor formation

Several aaRSs have come into the focus of cancer research (Kim et al., 2014). For instance, LeuRS senses the availability of the amino acid Leu and if these levels are sufficient to support growth, it signals a growth readiness to the key growth controller TORC1/mTORC1 (Bonfils et al., 2012; Han et al., 2012). Our results suggest that PheRS does not serve an analogous function as a Phe sensor (Suppl. Figure S3). Phe binding appears to be dispensable to activate proliferation and to repress *Notch* signaling because the α-PheRS^{Cys} mutant, in which two essential residues in the Phe binding pocket were replaced by Cys is unable to perform

aminoacylation (presumably because it cannot bind Phe), but still able to induce the non-canonical activity.

Improper expression of PheRS was suspected long ago to promote carcinogenesis, but till now the mechanisms behind this effect remind unknown. Elevated levels of *FARSA/CML33* (human α-PheRS) during the development of myeloid leukemia have been demonstrated to directly correlate with tumorigenic events (Sen et al., 1997). The GENT database published in 2011 describes also strong positive correlations between PheRS subunit levels and tumorigenic events in several tissues and cancers, including colon cancer, which mostly seems to originate from intestinal stem cells (ISCs) (Barker et al., 2009). Modelling the effect of elevated α-PheRS levels in *Drosophila* ISCs and CBs, we found that these levels lead to over-proliferation of cells with stem cell characteristics and to changes in cell fate, indicating that elevated α-PheRS levels can indeed be a risk factor for tumor formation.

Modeling the effects of elevated α-PheRS levels in ISCs revealed that hyperaccumulation of stem cells, a tumor risk, is mediated by high α-PheRS repressing Notch signaling. In mammals, Notch signaling is essential for maintaining the homeostasis of cell proliferation and differentiation (Qiao and Wong, 2009) similar to the function of Notch signaling in the Drosophila gut that is needed to prevent the induction of enteroendocrine tumors characterized by excessive EEs and ISCs in the adult midgut (Micchelli and Perrimon, 2006; Ohlstein and Spradling, 2007). Because in human, mis-regulation of Notch signaling in these processes has been suggested to trigger the development of colon cancer, *Notch* has been proposed as a molecular target for cancer therapy (Yin et al., 2010). The results presented here provide new and unexpected insights into the communication between two major signaling pathways involved in gut tumorigenesis and they suggest new opportunities to target these mechanisms.

Materials and Methods

Key Resources Table

Reagent or Resource	Sources	Identifier	Additional information
Antibodies			
Anti phospho-Histone H3-rabbit	Cell signaling	9701S	1:200 v/v
Anti phospho-Histone H3-mouse	Cell signaling	9706S	1:200 v/v
Anti *α-PheRS*	Genescript	4668	Customized product (1:200 v/v)
Anti *α-PheRS*	Genescript	4669	Customized product (1:200 v/v)
Anti Myc-mouse	Developmental Studies Hybridoma Bank (DSHB)	9E10	Supernatant (1:3 v/v)
Anti Puromycin	DSHB	PMY-2A4	1:100 v/v
Anti Prospero	DSHB	MR1A	1:200 v/v
Anti Delta	DSHB	C594.9B	1:10 v/v
Anti V5 tag-rabbit	Cell signaling	13202	1:200 v/v
Anti Cy3 rabbit	Jackson Immuno Research	115-165-146	1:200 v/v
Anti-rabbit Alexa Flour 488	Molecular Probes	A-11008	1:200 v/v
Anti-rabbit Alexa Flour 488	Molecular Probes	A-11034	1:200 v/v
Anti-mouse Alexa Flour 488	Molecular Probes	A-11029	1:200 v/v
Anti-rabbit Alexa Flour 488	Life technology	A-21206	1:200 v/v
Anti-rabbit Alexa Flour 594	Invitrogen	A-11037	1:200 v/v
Anti-mouse Alexa Flour 594	Molecular Probes	A-11032	1:200 v/v
Anti-mouse Alexa Flour 568	Life technology	A-10037	1:200 v/v
Anti α-tubulin	Abcam	Ab18251	1:1,000 v/v
Anti GFP	ImmunoKontact	042704	1:1,000 v/v
Anti Myc-rabbit	Santa Cruz	Sc-789	A-12 (1:1,000 v/v)
HRP Anti rabbit IgG antibody (Peroxidase)	Vector	PI-1000	1:10,000 v/v
HRP Anti rabbit IgG antibody (Peroxidase)	Vector	PI-2000	1:10,000 v/v

Fly stocks and genetics			
α-PheRS^{G2060}/FM6	Bloomington Drosophila Stock Center (BDSC)	26625	
RNAi- α-PheRS	Vienna Drosophila RNAi Center (VDRC)	33514	
RNAi- β-PheRS	VDRC	42046	
eyeless-Gal4	BDSC	5535	
engrailed-Gal4	BDSC	30564	
UAS-GFP	BDSC	6658	
STAT92E[HJ]/TM3,Sb	BDSC	24510	
w; UAS-Myc::MYC	BDSC	9674	
hspFLP/y ; + ; UAS-Myc::MYC	BDSC	9675	
hspFLP/y ; UAS-N^{ICD} /CyO ; MKRS/TM2	BDSC	52008	
10X STAT92E GFP	BDSC	26197	
UAS-N RNAi	BDSC	33611	
UAS-N RNAi	BDSC	7078	
*neoFRT*82B *Sb1*/TM6	BDSC	2051	
NRE-EGFP	BDSC	30728	
UAS-Dl	BDSC	5614	
tub-Gal4/TM3,Sb	BDSC	5138	
y w att2A[vas-ϕ]; +; attP-86F	ETH Zurich		A gift from Hugo Stocker, ETH
esg-Gal4,UAS-2XEYFP;MKRS/TM6B,Tb	ETH Zurich		A gift from Hugo Stocker, ETH
yw; esg-Gal4, UAS-GFP/TM6B,Tb,Hu	ETH Zurich	2400	A gift from Hugo Stocker, ETH
NP1-Gal4 (Myo31DF)/CyO y+	ETH Zurich	2398	A gift from Hugo Stocker, ETH
esg-Gal4, UAS-mCherry-CD8, tub-gal80^{ts}/CyO			A gift from Péter Nagy, Cornell University
yw;UAS-cyto-gars-myc/CyO			A gift from Albena Jordanova, VIB-U Antwerp Center for Molecular Neurology

Bacteria strains and vectors		
XL1 blue	Aligent	200249
Rosseta – Novagen	Merckmilipore	70954
pET-28a – Novagen	Merckmilipore	69864
pET LIC (2A-T)	Addgene	29665
pUASattB	Drosophila Genomics Resource Center	1419
pw+SNattB	(Koch et al., 2009)	
Commercial assay or kit		
Pierce® Silver Stain kit	Thermo Scientific	24612
Pierce® BCA Protein Assay kit	Thermo Scientific	23227
ReliaPrep™ DNA CleanUp and Concentration System	Promega	A2893
GeneElute™ HP Plasmid miniprep kit	Sigma	NA0160
Qiagen® Plasmid Plus Midi kit	Qiagen	12943
Ni-NTA affinity resin	Qiagen	30210
ECL™ Prime Western Blotting System	GE Healthcare	RPN2232
RNAMaxx™ High Yield Transcription Kit	Aligent	200339
Software, algorithm		
Leica Application Suite X (LAS X)	Leica	https://www.leica-microsystems.com/products/microscope-software/p/leica-las-x-ls/
FIJI	ImageJ	https://fiji.sc/
GraphPad Prism	GraphPad	https://www.graphpad.com/scientific-software/prism/
FlowJo™	BD Biosciences	https://www.flowjo.com/
Microsoft Excel	Microsoft	https://products.office.com/en-us/excel

Buffers

Lysis buffer for Drosophila tissue	**Lysis buffer for bacteria**
20 mM Tris HCl pH7.4 150uM NaCl 2 mM EDTA 50 mM NaF 10% Glycerol 1% Triton X100 1 Protease inhibitor cocktail tablet (Roche-4693159001)	20 mM Tris HCl pH7.4 150uM NaCl 2 mM EDTA 50 mM NaF 10% Glycerol 1% Triton X100 4mM Imidazole 1M 0.6% Lysozyme

1 mM phenylmethylsulphonyl fluoride	1 Protease inhibitor cocktail tablet 1 mM phenylmethylsulphonyl fluoride
4% PFA	**1X PBST**
1X PBST 4% (w/v) Paraformaldehyde	0.2 % (v/v) Tween 20 1X PBS
Blocking buffer	**Fly food recipe**
5% (w/v) non-fat dry milk 0.1% (v/v) Triton X100	20.4 l H_20 1,680 g Maize flour 720 g Yeast 1,800 g Syrup 192 g Potassium sodium tartrate tetrahydrate 36 g Nipagin 120 ml Propionic acid
10X PBS pH 7.4	
10.6 mM KH_2PO_4 1.5 M NaCl 30 mM $Na_2PO_4.7H_20$	
10X SDS running buffer	**10X Transfer buffer**
30 g Tris base 144 g Glycine 10 g SDS dH_2O to 1ℓ	30 g Tris base 144 g Glycine dH_2O to 1ℓ
10X TBS pH to 7.6	**1X TBST**
24 g of Tris Base 88 g of NaCl dH_2O to 1ℓ	100 mL 10X TBS 900 mL dH_2O 0.1% (v/v) Tween 20

Primers

Name	**Sequence (5' to 3')**	**Application**
rc2263f	CGCGGATCCATCCGGCGAGAGAGTGTCTTTG	Genomic genomic construct of *α-PheRS*
rc2263r	CGGGGTACCTATGCCTGGCGATAATCGTG	
Tyr412Cys & Phe438Cys-F	TCAAGCCGGCGTACAATCCGTGTACCGAGCCCAG	Construct of *α-PheRS*^{Cys} mutation
Tyr412Cys & Phe438Cys-R	CTCCGGCCGACAGACGCCCGAGTTGCCC	
α-PheRS RNAi 11f	TAATACGACTCACTATAGGGAGGCAAGAAACGCAAGCTCCTC	*α-PheRS* ds RNA synthesis
α-PheRS RNAi 11r	TAATACGACTCACTATAGGGAGGGAACTCCGCCAGATGTGTG	
β-PheRS RNAi 10f	TAATACGACTCACTATAGGGAGGGCCAATCATTCGGGAATCA	*β-PheRS* ds RNA synthesis
β-PheRS RNAi 10r	TAATACGACTCACTATAGGGAGGAGGCAGGGACTTCTTAATGT	
seq r6	GCTCCCATTCATCAGTTCC	Sequencing
seqA r1	CATTTCCACCGTGAGATCCGTC	Sequencing
seqA r2	AACTCTTGTGGGTGACCGTTTC	Sequencing
seqA f1	GTTCTCGAAGTGAATGTTCTGG	Sequencing

seqA f2	TTTAGCCACCGTCGTCGTTTC	Sequencing
seqA r3	TCCAGCGACGATGACGAATTTG	Sequencing
seqA f3	CAAATGGATTGTGGGACCAGC	Sequencing
seqA r4	GCCCTCCTCCACCATCTTTAG	Sequencing

Fly genetics and husbandry

All *Drosophila melanogaster* fly stocks were kept for long term storage at 18ºC in glass or plastic vials on standard food with day/night (12h/12h) light cycles. All experiments were performed at 25ºC unless specifically mentioned. A UAS-GFP element was added in the crosses of all rescue experiments to even out the effect of Gal4 by providing the same number of UAS constructs. Origins of all stocks are noted in the *Key Resource Table*.

DNA cloning and generation of transgenic flies

Sequence information was obtained from Flybase. All mutations and the addition of the Myc-tag to the N-terminus of *α-PheRS* were made by following the procedure of the QuickChange® Site-Directed Mutagenesis Kit (Stratagene). The genomic *α-PheRS* rescue construct (*Myc::α-PheRS*) codes for the entire coding region and for an additional Myc tag at the N-terminal end. In addition, it contains ~ 1kb of up- and down-stream sequences and it was cloned into the *pw*$^{+}$*SNattB* transformation vector (Koch et al., 2009; Lu et al., 2014). The *α-PheRS* and *β-PheRS* cDNAs were obtained by RT-PCR from mRNA isolated from 4-8 days old *OreR* flies (Lu et al., 2014). The Tyr412Cys and Phe438Cys mutations in the *α-PheRS* sequence were created by site directed mutagenesis. Like the wild-type cDNA, they were cloned into the *pUASTattB* transformation vector to generate the pUAS-α-PheRS and pUAS-α-PheRS^{Cys}. Before injecting these constructs into fly embryos, all plasmids were verified by sequencing (Microsynth AG, Switzerland). Transgenic flies were generated by applying the *ϕ* C31-based integration system with the stock (*y w att2A[vas-ϕ]; +; attP-86F*) (Bischof et al., 2007).

Western blotting

Protein was extracted from tissues, whole larvae, or flies using the lysis buffer. Protein lysates were separated by SDS-PAGE and transferred onto PVDF membranes (Milipore, US). The blocking was performed for 1h at room temperature (RT) with non-fat dry milk (5%) in TBST solution. Blots were probed first with primary antibodies (diluted in blocking buffer) overnight at 4°C and then with secondary antibodies (diluted in TBST) 1h at RT. The signal of the secondary antibody was detected by using the detect solution mixture (1:1) (ECL™ Prime Western Blotting System, GE Healthcare Life Science) and a luminescent detector (Amersham Imager 600, GE Healthcare Life Science). Origins and recipes of all buffers and reagents are noted in *Key Resource Table*.

Immunofluorescent staining and confocal microscopy

Guts were dissected from each female fly 3 days after eclosure, and a total of 10 guts were analyzed for each genotype. Dissections were performed in PBS 1X on ice and tissues were collected within maximum one hour. Fixation with 4% PFA in PBS-T 0.2% at RT was done for different durations depending on the different tissues: two hours (gut), 40 minutes (brain), 30 minutes (wing discs, ovary). Then the samples were blocked overnight with blocking buffer at 4°C. Primary antibodies (diluted in blocking buffer) were incubated with the samples for 8h at RT. The samples were rinsed 3 times and washed 3 times (20 minutes/wash) with PBST. Secondary antibodies (diluted in PBST) were incubated overnight at 4°C. The samples were then rinsed 3 times and washed 2 times (20 minutes/wash) with PBST. Hoechst 33258 (2.5 μg/ml) was added in PBST before the last washing step and the samples were mounted with Aqua/Poly Mount solution (Polysciences Inc., US). For the anti-Delta labeling, the samples

were blocked for 3h at RT with blocking buffer. The primary anti-Delta antibody (1:10 v/v) was incubated with the samples overnight at 4ºC and then the secondary antibody was incubated overnight at 4ºC. Origins and diluted concentrations of all buffers and antibodies are noted in *Key Resource Table*.

Protein synthesis measurements using the ribopuromycylation method (RPM)

For puromycin labeling experiments, tissues were dissected in Schneider's insect medium (Sigma, US) supplement with 10% fetal calf serum (FCS, Sigma, US) at 25ºC. They were then incubated with Schneider's insect medium containing puromycin (5 µg/ml, Sigma, US) and cycloheximine (CHX, 100 µg/ml, Sigma, US) for 2 hours at RT. Then the samples were fixed with 4% PFA in PBS-T 0.2% at RT and blocked overnight with blocking buffer at 4ºC. Primary anti-Puromycin antibody (diluted in PBST) was incubated with the samples for 8h at RT. The samples were rinsed 3 times and washed 3 times (20 minutes/wash) with PBST. Secondary antibodies (diluted in PBST) were incubated overnight at 4ºC. The samples were then rinsed 3 times and washed 2 times (20 minutes/wash) with PBST. Hoechst 33258 (2.5 µg/ml) was added in PBST before the last washing step and the samples were mounted with Aqua/Poly Mount solution (Polysciences Inc., US).

***In vitro* aminoacylation assay**

Recombinant α-PheRS and β-PheRS proteins were expressed in the *E. coli* strain Rosetta (Novagen) and then purified (Moor et al., 2002). For this, the *α-PheRS* or *α-PheR*^{Cys} mutant cDNAs were cloned with His tags at the N-terminal end into the pET-28a plasmid expression vector (Novagen). Wild-type *β-PheRS* cDNAs were cloned into the pET LIC (2A-T) plasmid

(Addgene). Then, His-α-PheRS or the His-α-PheR^{Cys} mutant and β-PheRS were co-expressed in the *E. coli* strain Rosetta with isopropylthiogalactoside (IPTG, 1mM) induction at 25 °C for 6 hours. Proteins were purified with Ni-NTA affinity resin (Qiagen). The aminoacylation assay protocol from Jiongming Lu was then followed (Lu et al., 2014). This assay was performed at 25 °C in a 100μl reaction mixture containing 50 mM Tris-HCl pH 7.5, 10 mM $MgCl_2$, 4 mM ATP, 5 mM β-mercaptoethanol, 100 μg/ml BSA, 3 U/ml *E. coli* carrier tRNA, 5 μM [^{3}H]-amino acid (L-Phe) and 1 μM tRNA^{Phe} from brewer's yeast (Sigma, US). In each experiment, a 15-μl aliquot was removed at four different incubation time points, spotted on a Whatman filter paper discs and washed three times with ice-cold 5% trichloroacetic acid and once with ice-cold ethanol. A blank paper disc without spotting and another with spotting the enzyme-free reaction were used for detecting background signals. After filter discs were dried, they were immersed into PPO Toluol (Sigma, US) solution in plastic bottles and the radioactivity was measured by scintillation counting.

Wing disc dissociation and FACS analysis

Wandering larvae derived from 2-4 hours egg collections were dissected in PBS during a maximal time of 30 minutes. Around twenty wing discs were incubated with gentle agitation at 29°C for around 2-hours in 500μl 10× Trypsin-EDTA supplemented with 50 μl 10×Hank's Balanced Salt Solution (HBSS) (Sigma, US) and 10 μl Vybrant DyeCycle Ruby stain (Molecular Probes, US). Dissociated cells from wing discs were directly analyzed by FACS-Calibur flow cytometer (Becton Dickinson, US).

Drosophila tissue culture cells were harvested and fixed in 70% ethanol and stained with a staining solution containing 1mg/ml propidium iodide, 0.1% Triton and 10 mg/ml RNase A. The cells were then subjected to FACS-Calibur cytometry and data were analyzed with the FlowJo software.

Drosophila cell culture and RNAi treatment

The protocols for in vitro cell culture and RNAi treatment was described in the PhD thesis of Jiongming Lu (Lu, 2013). *Drosophila* Kc cells were incubated at 25°C in Schneider's *Drosophila* medium supplemented with 10% heat-inactivated fetal calf serum (FCS) and 50 μg/ml Penicillin/Streptomycin. To induce RNAi knockdown in *Drosophila* cells, dsRNA treatment was performed (Clemens et al., 2000). dsRNAs around 500bp in length were generated with the RNAMaxx™ High Yield Transcription Kit (Agilent, US). Cells were diluted to a concentration of 10^6 cells/ml in serum-free medium, and dsRNA was added directly to the medium at a concentration of 15 μg/ml. The cells were incubated for 1 hour followed by addition of medium containing FCS. Then the cells were kept in the incubator and were harvested at different time points (1-5 days) after dsRNA treatment.

Clonal assay and twin spot data analysis

For twin spot tests, we used the Mosaic Analysis with a Repressible Cell Marker (MARCM) system. Twin spots were generated with the progenitor genotype *hs-flp; tub-Gal4/UAS-β-PheRS ; FRT82B, ubiGFP, UAS-α-PheRS$^{(Cys)}$/FRT82B Tub-Gal80.* In twin spots, the internal control clone was GFP-minus and the sister clone with the red signal generated by the antibody against the overexpressed protein. We induced the *hs-FLP*, *FRT82B* system at 37°C for 1h on the third day post-eclosure and dissected the animals 3 days post-induction. Confocal imaging detected non-green clones (without ubiGFP) and red clones (stained with Myc antibody-red) (Fig 9A).

In twin spots, cell numbers per clone were counted and the numbers of cell division per clone were calculated as $\log_2$(cell numbers per clone). This represents the logarithm of the cell numbers per clone to the base 2. The increase of cell proliferation (%) was analyzed by comparing the number of cell divisions of the two clones in the same twin spot.

Image acquisition and processing

Imaging was carried out with a Leica SP8 confocal laser scanning microscope equipped with a 405 nm diode laser, a 458, 476, 488, 496 and 514 nm Argon laser, a 561 nm diode pumped solid state laser and a 633 nm HeNe laser. Images were obtained with 20x dry and 63x oil-immersion objectives and 1024x1024 pixel format. Images were acquired using LAS X software. The images of the entire gut were obtained by imaging at the standard size and then merging maximal projections of Z-stacks with the Tiles Scan tool. Fluorescent intensity was determined from FIJI software.

Quantification of cell numbers per posterior midgut

Z stack images through the width of the posterior midgut were acquired along the length of the posterior midgut from the R4a compartment to midgut-hindgut junction. Maximum projections of each Z stack were obtained, and the total number of each cell type was counted manually and exported to Microsoft Excel and GraphPad Prism for further statistical analysis.

Quantification and statistical analysis

For quantifications of all experiments, *n* represents the number of independent biological samples analyzed (the number of guts, the number of wing disc, the number of twin spots), error bars represent standard deviation (SD). Statistical significance was determined using the

t-test or ANOVA as noted in the figure legends. They were expressed as P values. (*) denotes $p < 0.05$, (**) denotes $p < 0.01$, (***) denotes $p < 0.001$, (****) denotes $p < 0.0001$. (*ns*) denotes values whose difference was not significant.

Acknowledgements

We thank Peter Nagy, Hugo Stocker, Albena Jordanova, Erik Storkebaum and the Bloomington Stock Center for fly stocks. We are also grateful to Mark Safro for suggesting mutations that disrupt the phenylalanine binding site of α-PheRS. This work was supported by the Novartis Foundation for medical-biological Research (#18A050), the Swiss National Fund (project grant 31003A_173188) and the University/Canton of Bern.

References

Ables, J.L., Breunig, J.J., Eisch, A.J., Rakic, P., 2011. Not(ch) just development: Notch signalling in the adult brain. Nature reviews. Neuroscience 12, 269-283.

Adam, I., Dewi, D.L., Mooiweer, J., Sadik, A., Mohapatra, S.R., Berdel, B., Keil, M., Sonner, J.K., Thedieck, K., Rose, A.J., Platten, M., Heiland, I., Trump, S., Opitz, C.A., 2018. Upregulation of tryptophanyl-tRNA synthethase adapts human cancer cells to nutritional stress caused by tryptophan degradation. Oncoimmunology 7, e1486353.

Antonellis, A., Oprescu, S.N., Griffin, L.B., Heider, A., Amalfitano, A., Innis, J.W., 2018. Compound heterozygosity for loss-of-function FARSB variants in a patient with classic features of recessive aminoacyl-tRNA synthetase-related disease. Human mutation 39, 834-840.

Bach, E.A., Ekas, L.A., Ayala-Camargo, A., Flaherty, M.S., Lee, H., Perrimon, N., Baeg, G.H., 2007. GFP reporters detect the activation of the Drosophila JAK/STAT pathway in vivo. Gene expression patterns : GEP 7, 323-331.

Barker, N., Ridgway, R.A., van Es, J.H., van de Wetering, M., Begthel, H., van den Born, M., Danenberg, E., Clarke, A.R., Sansom, O.J., Clevers, H., 2009. Crypt stem cells as the cells-of-origin of intestinal cancer. Nature 457, 608-611.

Bina, S., Wright, V.M., Fisher, K.H., Milo, M., Zeidler, M.P., 2010. Transcriptional targets of Drosophila JAK/STAT pathway signalling as effectors of haematopoietic tumour formation. EMBO reports 11, 201-207.

Bischof, J., Maeda, R.K., Hediger, M., Karch, F., Basler, K., 2007. An optimized transgenesis system for Drosophila using germ-line-specific phiC31 integrases. Proceedings of the National Academy of Sciences of the United States of America 104, 3312-3317.

Bonfils, G., Jaquenoud, M., Bontron, S., Ostrowicz, C., Ungermann, C., De Virgilio, C., 2012. Leucyl-tRNA synthetase controls TORC1 via the EGO complex. Molecular cell 46, 105-110.

Buchon, N., Broderick, N.A., Chakrabarti, S., Lemaitre, B., 2009. Invasive and indigenous microbiota impact intestinal stem cell activity through multiple pathways in Drosophila. Genes & development 23, 2333-2344.

Casas-Tinto, S., Lolo, F.N., Moreno, E., 2015. Active JNK-dependent secretion of Drosophila Tyrosyl-tRNA synthetase by loser cells recruits haemocytes during cell competition. Nature communications 6, 10022.

Chen, J., Larochelle, S., Li, X., Suter, B., 2003. Xpd/Ercc2 regulates CAK activity and mitotic progression. Nature 424, 228-232.

Clemens, J.C., Worby, C.A., Simonson-Leff, N., Muda, M., Maehama, T., Hemmings, B.A., Dixon, J.E., 2000. Use of double-stranded RNA interference in Drosophila cell lines to dissect signal transduction pathways. Proceedings of the National Academy of Sciences 97, 6499-6503.

de la Pompa, J.L., Wakeham, A., Correia, K.M., Samper, E., Brown, S., Aguilera, R.J., Nakano, T., Honjo, T., Mak, T.W., Rossant, J., Conlon, R.A., 1997. Conservation of the Notch signalling pathway in mammalian neurogenesis. Development 124, 1139-1148.

Deliu, L.P., Ghosh, A., Grewal, S.S., 2017. Investigation of protein synthesis in Drosophila larvae using puromycin labelling. Biology open 6, 1229-1234.

Dolde, C., Lu, J., Suter, B., 2014. Cross Talk between Cellular Regulatory Networks Mediated by Shared Proteins. Advances in Biology 2014, 12.

Finarov, I., Moor, N., Kessler, N., Klipcan, L., Safro, M.G., 2010. Structure of human cytosolic phenylalanyl-tRNA synthetase: evidence for kingdom-specific design of the active sites and tRNA binding patterns. Structure 18, 343-353.

Giachino, C., Taylor, V., 2014. Notching up neural stem cell homogeneity in homeostasis and disease. Frontiers in neuroscience 8, 32.

Gomard-Mennesson, E., Fabien, N., Cordier, J.F., Ninet, J., Tebib, J., Rousset, H., 2007. Clinical significance of anti-histidyl-tRNA synthetase (Jo1) autoantibodies. Annals of the New York Academy of Sciences 1109, 414-420.

Grandbarbe, L., Bouissac, J., Rand, M., Hrabe de Angelis, M., Artavanis-Tsakonas, S., Mohier, E., 2003. Delta-Notch signaling controls the generation of neurons/glia from neural stem cells in a stepwise process. Development 130, 1391-1402.

Greenberg, Y., King, M., Kiosses, W.B., Ewalt, K., Yang, X., Schimmel, P., Reader, J.S., Tzima, E., 2008. The novel fragment of tyrosyl tRNA synthetase, mini-TyrRS, is secreted to induce an angiogenic response in endothelial cells. FASEB journal : official publication of the Federation of American Societies for Experimental Biology 22, 1597-1605.

Guo, M., Schimmel, P., 2013. Essential nontranslational functions of tRNA synthetases. Nature chemical biology 9, 145-153.

Han, J.M., Jeong, S.J., Park, M.C., Kim, G., Kwon, N.H., Kim, H.K., Ha, S.H., Ryu, S.H., Kim, S., 2012. Leucyl-tRNA synthetase is an intracellular leucine sensor for the mTORC1-signaling pathway. Cell 149, 410-424.

Hariharan, I.K., 2015. Organ Size Control: Lessons from Drosophila. Developmental cell 34, 255-265.

Hatakeyama, J., Bessho, Y., Katoh, K., Ookawara, S., Fujioka, M., Guillemot, F., Kageyama, R., 2004. Hes genes regulate size, shape and histogenesis of the nervous system by control of the timing of neural stem cell differentiation. Development 131, 5539-5550.

Herrera, S.C., Bach, E.A., 2019. JAK/STAT signaling in stem cells and regeneration: from Drosophila to vertebrates. Development 146.

Housden, B.E., Millen, K., Bray, S.J., 2012. Drosophila Reporter Vectors Compatible with PhiC31 Integrase Transgenesis Techniques and Their Use to Generate New Notch Reporter Fly Lines. G3 (Bethesda) 2, 79-82.

Jiang, H., Patel, P.H., Kohlmaier, A., Grenley, M.O., McEwen, D.G., Edgar, B.A., 2009. Cytokine/Jak/Stat signaling mediates regeneration and homeostasis in the Drosophila midgut. Cell 137, 1343-1355.

Kim, D., Kwon, N.H., Kim, S., 2014. Association of aminoacyl-tRNA synthetases with cancer. Topics in current chemistry 344, 207-245.

Ko, Y.G., Kang, Y.S., Kim, E.K., Park, S.G., Kim, S., 2000. Nucleolar localization of human methionyl-tRNA synthetase and its role in ribosomal RNA synthesis. The Journal of cell biology 149, 567-574.

Ko, Y.G., Kim, E.Y., Kim, T., Park, H., Park, H.S., Choi, E.J., Kim, S., 2001. Glutamine-dependent antiapoptotic interaction of human glutaminyl-tRNA synthetase with apoptosis signal-regulating kinase 1. The Journal of biological chemistry 276, 6030-6036.

Koch, R., Ledermann, R., Urwyler, O., Heller, M., Suter, B., 2009. Systematic functional analysis of Bicaudal-D serine phosphorylation and intragenic suppression of a female sterile allele of BicD. PloS one 4, e4552.

Korzelius, J., Naumann, S.K., Loza-Coll, M.A., Chan, J.S., Dutta, D., Oberheim, J., Glasser, C., Southall, T.D., Brand, A.H., Jones, D.L., Edgar, B.A., 2014. Escargot maintains stemness and suppresses differentiation in Drosophila intestinal stem cells. The EMBO journal 33, 2967-2982.

Laplante, M., Sabatini, D.M., 2012. mTOR signaling in growth control and disease. Cell 149, 274-293.

Lee, S.W., Cho, B.H., Park, S.G., Kim, S., 2004. Aminoacyl-tRNA synthetase complexes: beyond translation. Journal of cell science 117, 3725-3734.

Lin, G., Xu, N., Xi, R., 2010. Paracrine unpaired signaling through the JAK/STAT pathway controls self-renewal and lineage differentiation of drosophila intestinal stem cells. Journal of molecular cell biology 2, 37-49.

Ling, J., Yadavalli, S.S., Ibba, M., 2007. Phenylalanyl-tRNA synthetase editing defects result in efficient mistranslation of phenylalanine codons as tyrosine. RNA 13, 1881-1886.

Lu, J., 2013. Phenylalanyl tRNA synthetase: functions in and beyond aminoacylation, Institute of Cell Biology. University of Bern, Bern, Switzerland.

Lu, J., Bergert, M., Walther, A., Suter, B., 2014. Double-sieving-defective aminoacyl-tRNA synthetase causes protein mistranslation and affects cellular physiology and development. Nature communications 5, 5650.

Markowitz, S.D., Bertagnolli, M.M., 2009. Molecular origins of cancer: Molecular basis of colorectal cancer. The New England journal of medicine 361, 2449-2460.

Martin, F.A., Morata, G., 2006. Compartments and the control of growth in the Drosophila wing imaginal disc. Development 133, 4421-4426.

Micchelli, C.A., Perrimon, N., 2006. Evidence that stem cells reside in the adult Drosophila midgut epithelium. Nature 439, 475-479.

Moor, N., Linshiz, G., Safro, M., 2002. Cloning and expression of human phenylalanyl-tRNA synthetase in Escherichia coli: comparative study of purified recombinant enzymes. Protein expression and purification 24, 260-267.

Muller, P., Kuttenkeuler, D., Gesellchen, V., Zeidler, M.P., Boutros, M., 2005. Identification of JAK/STAT signalling components by genome-wide RNA interference. Nature 436, 871-875.

Nathanson, L., Deutscher, M.P., 2000. Active aminoacyl-tRNA synthetases are present in nuclei as a high molecular weight multienzyme complex. The Journal of biological chemistry 275, 31559-31562.

Niehues, S., Bussmann, J., Steffes, G., Erdmann, I., Kohrer, C., Sun, L., Wagner, M., Schafer, K., Wang, G., Koerdt, S.N., Stum, M., Jaiswal, S., RajBhandary, U.L., Thomas, U., Aberle, H., Burgess, R.W., Yang, X.L., Dieterich, D., Storkebaum, E., 2015. Impaired protein translation in Drosophila models for Charcot-Marie-Tooth neuropathy caused by mutant tRNA synthetases. Nature communications 6, 7520.

Ohlstein, B., Spradling, A., 2007. Multipotent Drosophila intestinal stem cells specify daughter cell fates by differential notch signaling. Science 315, 988-992.

Otani, A., Slike, B.M., Dorrell, M.I., Hood, J., Kinder, K., Ewalt, K.L., Cheresh, D., Schimmel, P., Friedlander, M., 2002. A fragment of human TrpRS as a potent antagonist of ocular angiogenesis. Proceedings of the National Academy of Sciences of the United States of America 99, 178-183.

Patel, P.H., Dutta, D., Edgar, B.A., 2015. Niche appropriation by Drosophila intestinal stem cell tumours. Nature cell biology 17, 1182-1192.

Qiao, L., Wong, B.C., 2009. Role of Notch signaling in colorectal cancer. Carcinogenesis 30, 1979-1986.

Roy, H., Ibba, M., 2006. Phenylalanyl-tRNA synthetase contains a dispensable RNA-binding domain that contributes to the editing of noncognate aminoacyl-tRNA. Biochemistry 45, 9156-9162.

Schimmel, P.R., Soll, D., 1979. Aminoacyl-tRNA synthetases: general features and recognition of transfer RNAs. Annual review of biochemistry 48, 601-648.

Sen, S., Zhou, H., Ripmaster, T., Hittelman, W.N., Schimmel, P., White, R.A., 1997. Expression of a gene encoding a tRNA synthetase-like protein is enhanced in tumorigenic human myeloid leukemia cells and is cell cycle stage- and differentiation-dependent. Proceedings of the National Academy of Sciences of the United States of America 94, 6164-6169.

Smirnova, E.V., Lakunina, V.A., Tarassov, I., Krasheninnikov, I.A., Kamenski, P.A., 2012. Noncanonical functions of aminoacyl-tRNA synthetases. Biochemistry. Biokhimiia 77, 15-25.

Takashima, S., Adams, K.L., Ortiz, P.A., Ying, C.T., Moridzadeh, R., Younossi-Hartenstein, A., Hartenstein, V., 2011. Development of the Drosophila entero-endocrine lineage and its specification by the Notch signaling pathway. Developmental biology 353, 161-172.

Tzima, E., Reader, J.S., Irani-Tehrani, M., Ewalt, K.L., Schwartz, M.A., Schimmel, P., 2005. VE-cadherin links tRNA synthetase cytokine to anti-angiogenic function. The Journal of biological chemistry 280, 2405-2408.

Wang, C., Guo, X., Dou, K., Chen, H., Xi, R., 2015. Ttk69 acts as a master repressor of enteroendocrine cell specification in Drosophila intestinal stem cell lineages. Development 142, 3321-3331.

Wang, H., Chen, X., He, T., Zhou, Y., Luo, H., 2013. Evidence for tissue-specific Jak/STAT target genes in Drosophila optic lobe development. Genetics 195, 1291-1306.

Wu, J.S., Luo, L., 2006. A protocol for mosaic analysis with a repressible cell marker (MARCM) in Drosophila. Nature protocols 1, 2583-2589.

Wullschleger, S., Loewith, R., Hall, M.N., 2006. TOR signaling in growth and metabolism. Cell 124, 471-484.

Yannay-Cohen, N., Carmi-Levy, I., Kay, G., Yang, C.M., Han, J.M., Kemeny, D.M., Kim, S., Nechushtan, H., Razin, E., 2009. LysRS serves as a key signaling molecule in the immune response by regulating gene expression. Molecular cell 34, 603-611.

Yin, C., Xi, R., 2018. A Phyllopod-Mediated Feedback Loop Promotes Intestinal Stem Cell Enteroendocrine Commitment in Drosophila. Stem cell reports 10, 43-57.

Yin, L., Velazquez, O.C., Liu, Z.J., 2010. Notch signaling: emerging molecular targets for cancer therapy. Biochemical pharmacology 80, 690-701.

Zhou, J.J., Wang, F., Xu, Z., Lo, W.S., Lau, C.F., Chiang, K.P., Nangle, L.A., Ashlock, M.A., Mendlein, J.D., Yang, X.L., Zhang, M., Schimmel, P., 2014. Secreted histidyl-tRNA synthetase splice variants elaborate major epitopes for autoantibodies in inflammatory myositis. The Journal of biological chemistry 289, 19269-19275.

Figure legends

Figure 1: *α–PheRS* overexpression increases numbers of mitotic cells without stimulating translation.

(A-B’’’,C) Wing disc phenotypes induced by the overexpression of α-*PheRS* or α-*PheRS*^{Cys}. *en-Gal4* was used to drive transgene expression in the posterior compartment of developing wing discs. Mitotic cells were labelled with anti-phospho-Histone H3 (PH3) antibodies (A: Anterior compartment/P: Posterior compartment). n=10, *p<0.05, **p<0.01 in t-test. (D-E”,F) Protein synthesis did not increase upon overexpression of *α-PheRS* or *α-PheRS* and *β-PheRS* together. *en-Gal4* was used to drive the overexpression of the transgenes in the posterior compartment of wing discs. dMyc was used as positive control. Protein synthesis was measured by the mean intensity of the puromycin (PMY) signal labelling the nascent polypeptides. n=15, ****p<0.0001, *ns:* not significant.

Figure 2: PheRS overexpression in wing discs induces excessive cell growth.

(A,B) PheRS overexpression increases wing size. One wing was chosen from each female fly, and a total of 20 wings were analyzed for each genotype. Quantification of wing size was performed by counting the pixels in both anterior (A) and posterior (P) compartments of the wing and calculating their ratio (P/A). PheRS overexpression of both subunits, but not a single subunit alone, increases wing size. GlyRS overexpression did not increase wing size, but slightly decreased it. Note that only the upper section of the y axis is shown. n=20, **, p<0.01 in t-test.

Figure 3: The proliferative activity of the *α-PheRS* subunit is independent of PheRS complex formation and tRNA^{Phe} aminoacylation.

Clonal analysis (twin spot) experiment of the effect of overexpression of the PheRS subunits in follicle cells by the MARCM technique. After inducing mitotic recombination by expressing the flipase under the control of the heat-shock (*hs*) promoter at 37°C for 40 minutes, a recombining cell will divide and give rise to two proliferating clones. (A) One clone (red) overexpresses PheRS and its twin clone (GFP^{-} signal) does not and expresses normal levels (internal control, outlined with yellow line). (B) Three days after inducing the recombination, the average number of cell divisions were calculated for each clone and compared to its twin spot to obtain the proliferation increase (%). n= 30, **p<0.01, ***p<0.001, ****p<0.0001 in ANOVA test.

Figure 4: α-PheRS promotes ISC proliferation in the midgut.

(A) The number of ISC clusters increased upon overexpression of *Myc::α-PheRS* in ISCs and EBs (Esg^{+}-cells) of the larval gut. n=10, *p<0.05,****p<0.0001. (B) The cell number per Esg^{+} cluster increased upon overexpression of *Myc::α-PheRS* with the same *esg-Gal4* driver

used in (A). Esg^+ clusters were categorized according to the number of cells per cluster. The fraction of big clusters (cell number > 5) increased upon overexpression of *Myc::α-PheRS*. In contrast, the overexpression of *β-PheRS::V5* alone or the overexpression of *β-PheRS::V5* together with *Myc::α-PheRS* showed the same frequency of the different clusters as the wild type. (C-G) Whole gut images and pictures of the posterior midgut area (C'-G') showing the different cells observed. The expression of the different genes indicated were driven with the same driver used in (A). The EYFP signal (YFP) displayed in green marks ISCs and EBs, Hoechst (blue) stains the DNA in the nuclei. Overexpression of the $\alpha\text{-}PheRS^{Cys}$ mutant gave rise to tumor-like areas in both the anterior and the posterior midgut (outlined with dashed lines). (H) Mitotic cells were labelled with anti-phospho-Histone H3 (PH3) antibodies. n=10, ****p<0.0001 in t-test. (I) Total cells per intestinal region were measured by counting Hoechst 33258 labeled cells manually. n=10, ****p<0.0001. (J-J") The overexpression of *α-PheRS* or $\alpha\text{-}PheRS^{Cys}$ with the *esg-Gal4* driver in adult guts also resulted in an over-proliferation phenotype of Esg^+ stem cells and progenitor cells.

Figure 5: Elevated α-PheRS levels increase EE differentiation in the gut through downregulating Notch signaling.

(A-B,C) Overexpression of $\alpha\text{-}PheRS^{Cys}$ using the *esg-Gal4,UAS-2XEYFP* system led to an increase in the number of EEs compared to the ECs in both larval and adult guts. EEs were marked by anti-Prospero antibody, Hoechst-labelled polyploid cells were counted as ECs. Guts were dissected from female flies 3 days after eclosure, and at least 10 guts were analyzed for each genotype. n=10, ****p<0.0001. (A",B") The co-overexpression of $\alpha\text{-}PheRS^{Cys}$ with *Notch* rescued the over-proliferation of Esg^+ cells as well as the EE/EC ratio.

(D-E') Whole adult gut images (D,E) and the posterior midgut area (D',E'). The same *esg-Gal4* driver marks ISCs and EBs (EYFP signal shown in green), Hoechst (blue) stains nuclear DNA. The *Notch* knockdown phenotype in the posterior midgut (outlined with dashed lines) is indistinguishable from the $\alpha\text{-}PheRS^{Cys}$ overexpression phenotype. Co-overexpression of $\alpha\text{-}PheRS^{Cys}$ with *Notch* rescued the midgut phenotype. (F) Notch activity reporter (NRE-EGFP) levels drastically decrease upon *α-PheRS* or $\alpha\text{-}PheRS^{Cys}$ overexpression in adult midgut ISCs that expresses GFP under the control of a Notch response element (NRE). The guts were dissected from female flies 3 days after eclosure. Protein lysates were then extracted and separated by SDS-PAGE gel. 25 guts were analyzed for each genotype.

Figure 6: High levels of *α-PheRS* repress neuroblast proliferation by downregulating the *Notch* pathway.

(A-A") The overexpression of *α-PheRS* or $\alpha\text{-}PheRS^{Cys}$ in neuroblasts reduced the ratio central brain (CB) size to optic lobe (OL) size. The *insc-Gal4,UAS-GFP* system was used to overexpress proteins in neuroblasts (NBs). NBs were labelled by GFP expression. Central brain (right area with GFP^+ NBs) and optic lobe area (left) are distinguished by a white

dashed line. (B) Effect of overexpression and knock down of *α-PheRS*$^{(Cys)}$and *Notch* on the CB/OL size ratio. n=20, ***p<0.001, *ns*: not significant. (C) The larval brains were dissected from third instar larvae, and at least 20 brains were analyzed for each genotype. Each brain lobe was classified according to the number of type II NBs per brain lobe. The overexpression of *α-PheRS* or *α-PheRS*^{Cys} reduced the number of type II NBs per brain lobe, and less than half of the lobes contained the normal 7-8 NBs. *Notch RNAi* caused the same phenotype with higher expressivity. Overexpressing *Notch* together with *α-PheRS*^{Cys} rescued the loss of NB phenotype to normal wild-type levels. n = 25.

Figure 7: The JAK/STAT transcription factor STAT92E regulates α-PheRS levels.

(A-C'') Hypomorphic *Stat92E*^{HJ} mutants contain high levels of α-PheRS in their ISCs (B). Anti-Delta antibody was used to label ISCs, and anti-α-PheRS was used to stain for α-PheRS. *esg-Gal4,UAS-2XEYFP* was used to drive YFP expression (A-A'', control) and *Stat92E* RNAi (C-C''), respectively, in ISCs and EBs. The white arrows indicate polyploid ECs with high levels of α-PheRS. (D-F') The quantification of the signal in the image (A",B",C") is based on the line across the nucleus of the cell. The signal intensity of α-PheRS differs between the ISC/EB (high) and distant EC (low) while the signal intensity of α-PheRS is similar between the ISC/EB (high) and the neighboring EC (high). (G) Suppressing the JAK/STAT signaling with the hypomorphic *Stat92E*^{HJ} allele or by RNAi significantly elevated the levels of α-PheRS in ISCs/EBs and neighboring ECs (Nb EC), but not in distant ECs. α-PheRS levels were measured by the mean intensity of the fluorescent signal. n=10, ****p<0.0001, *ns:* not significant. (H-I'') The overexpression of Stat92E decreased α-PheRS levels in Esg^{+} cells (circled with white dashed lines) in adult guts. The same setting was used as in (A). (J-K''') The *Stat92E* activity did not alter upon overexpression of α-PheRS. The *10X STAT92E-GFP* reporter was used to measure *Stat92E* activity. It expresses GFP under the control of ten STAT92E binding sites. The *esg-Gal4,UAS-mCD8:mCherry,tub-Gal80*^{ts} *system* was used to overexpress *α-PheRS* in ISCs and EBs. The female flies were collected 3 days after eclosure and cultured at 29°C for 7 days before dissecting and harvesting their midguts. (L-L"') The co-overexpression of *Stat92E* and *α-PheRS* with the *esg-Gal4* driver caused the same over-proliferative phenotype as *α-PheRS* overexpression alone, whereas *Stat92E* overexpression alone did not alter the Esg^{+} cell number. (M) *Stat92E* overexpression alone strongly increased levels of the Notch activity reporter (NRE-EGFP) in adult guts that express eGFP under the control of a Notch response element (NRE). In contrast, co-overexpression of *Stat92E* and *α-PheRS* reduced Notch activity down to 44% of the control levels, which is similar to the Notch activity levels observed upon overexpression of *α-PheRS* alone (41% of the wild-type levels). The guts were dissected from female flies 3 days after eclosure. Protein lysates were then extracted and separated by SDS-PAGE gel. 25 guts were analyzed for each genotype.

Figure 1

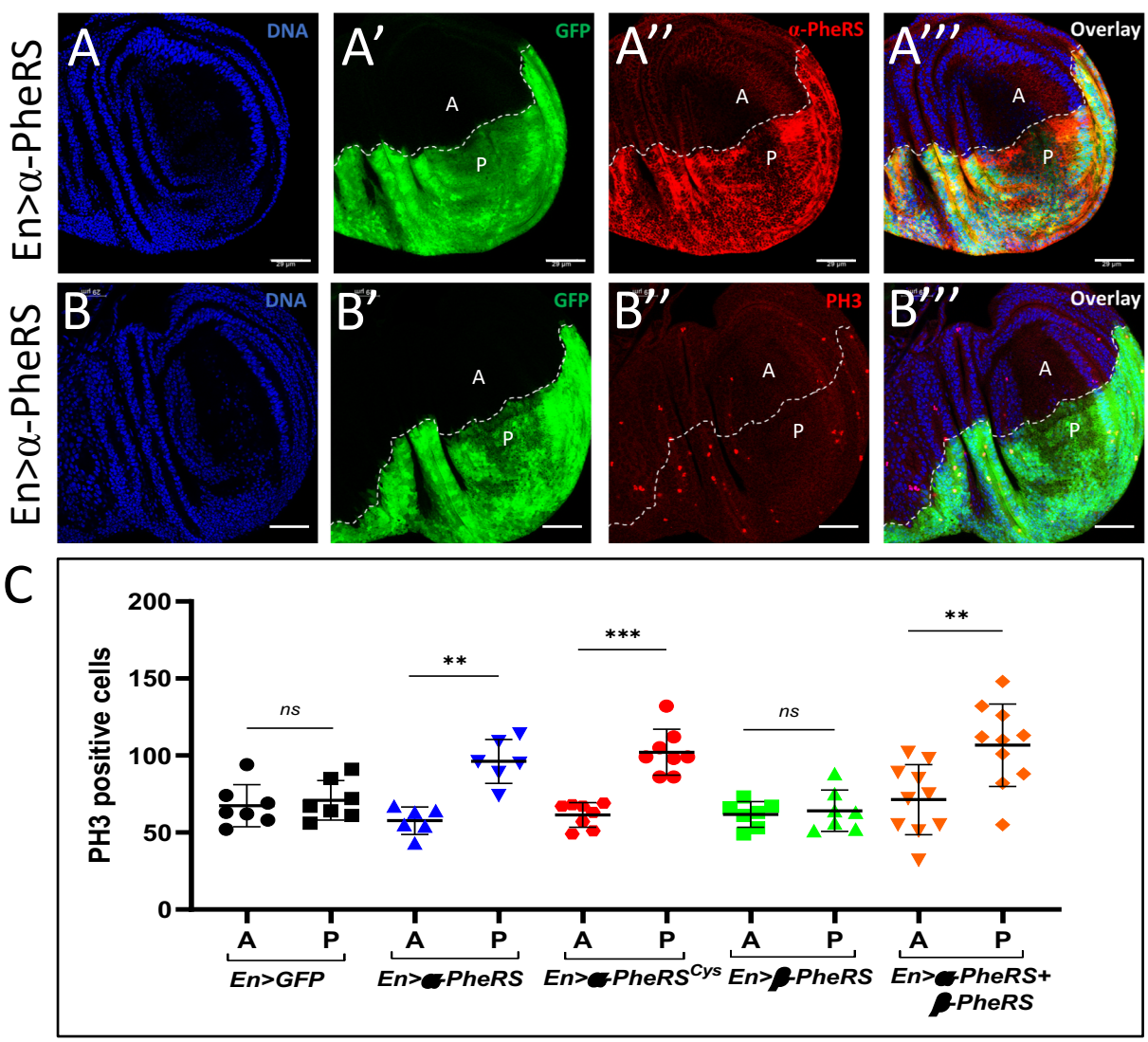
En>α-PheRS
A
DNA
A'
GFP
A''
α-PheRS
A'''
Overlay
A
P
En>α-PheRS
B
DNA
B'
GFP
B''
PH3
B'''
Overlay
C
PH3 positive cells
200
150
100
50
0
ns
**
***
ns
**
A
P
En>GFP
En>α-PheRS
En>α-PheRS^Cys
En>β-PheRS
En>α-PheRS+ β-PheRS

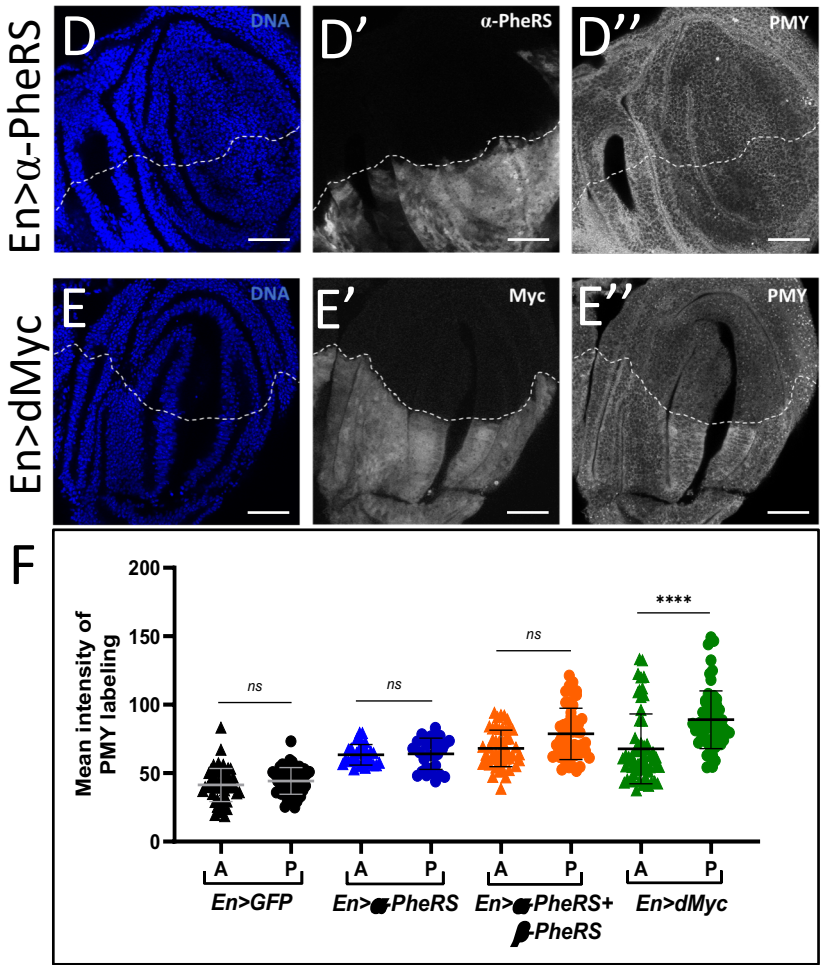
En>α-PheRS
D
DNA
D'
α-PheRS
D''
PMY
En>dMyc
E
DNA
E'
Myc
E''
PMY
F
Mean intensity of PMY labeling
200
150
100
50
0
ns
ns
ns
****
A
P
En>GFP
En>α-PheRS
En>α-PheRS+ β-PheRS
En>dMyc

Figure 2

A

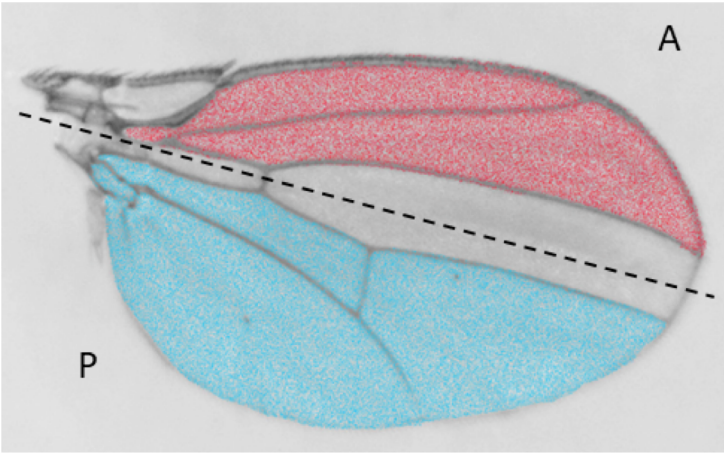
A
P

B

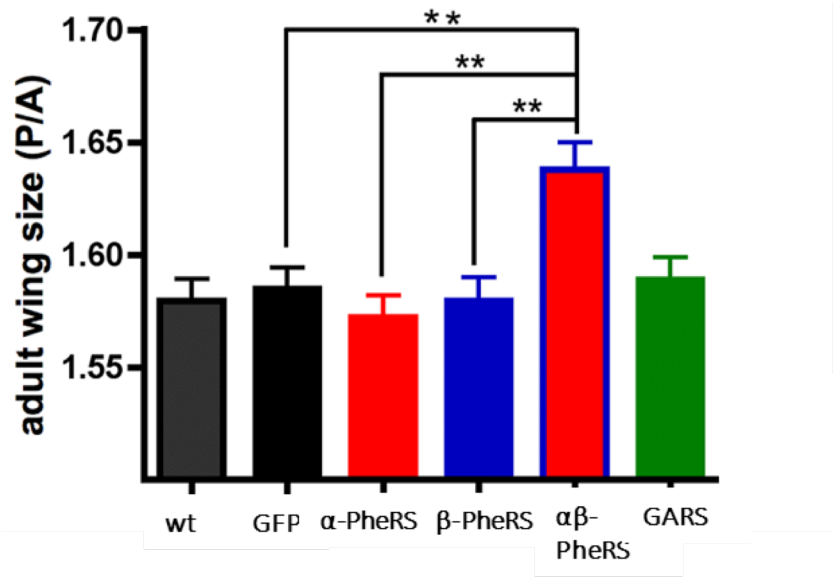
adult wing size (P/A)
1.70
1.65
1.60
1.55
**
**
**
wt
GFP
α-PheRS
β-PheRS
αβ-PheRS
GARS

Figure 3

A

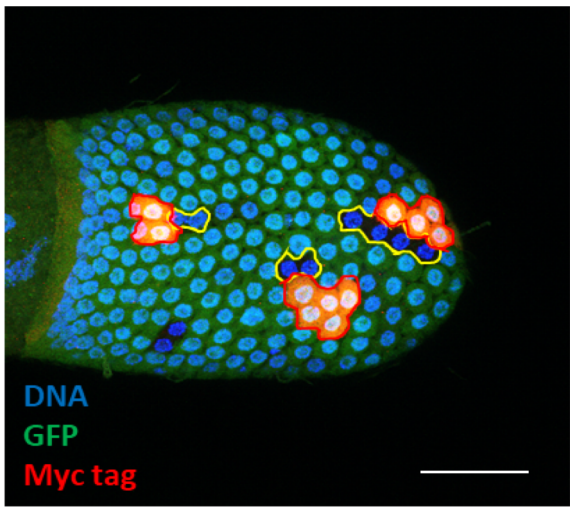
DNA
GFP
Myc tag

B

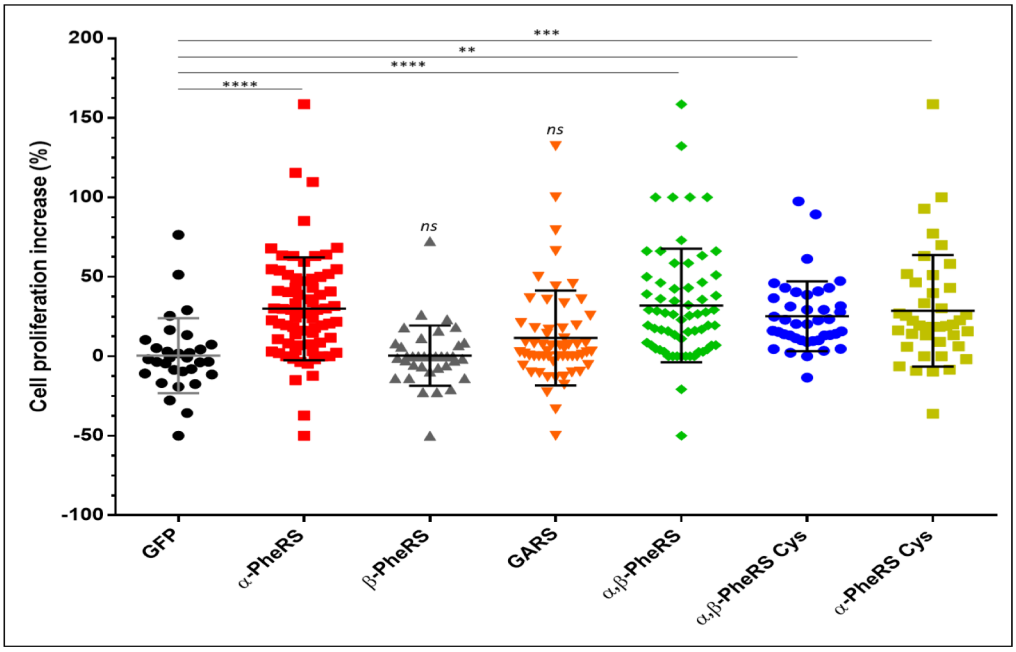
Cell proliferation increase (%)
200
150
100
50
0
-50
-100
***
**
****
****
ns
ns
GFP
α-PheRS
β-PheRS
GARS
α,β-PheRS
α,β-PheRS Cys
α-PheRS Cys

Figure 4

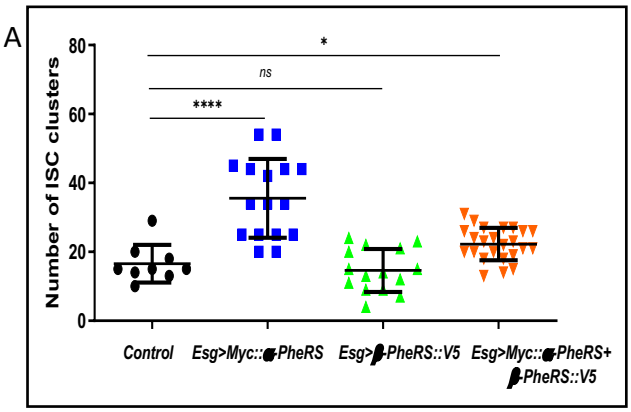

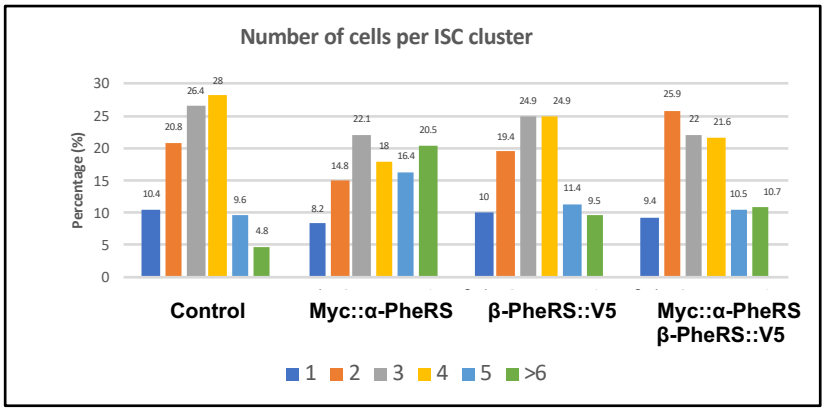

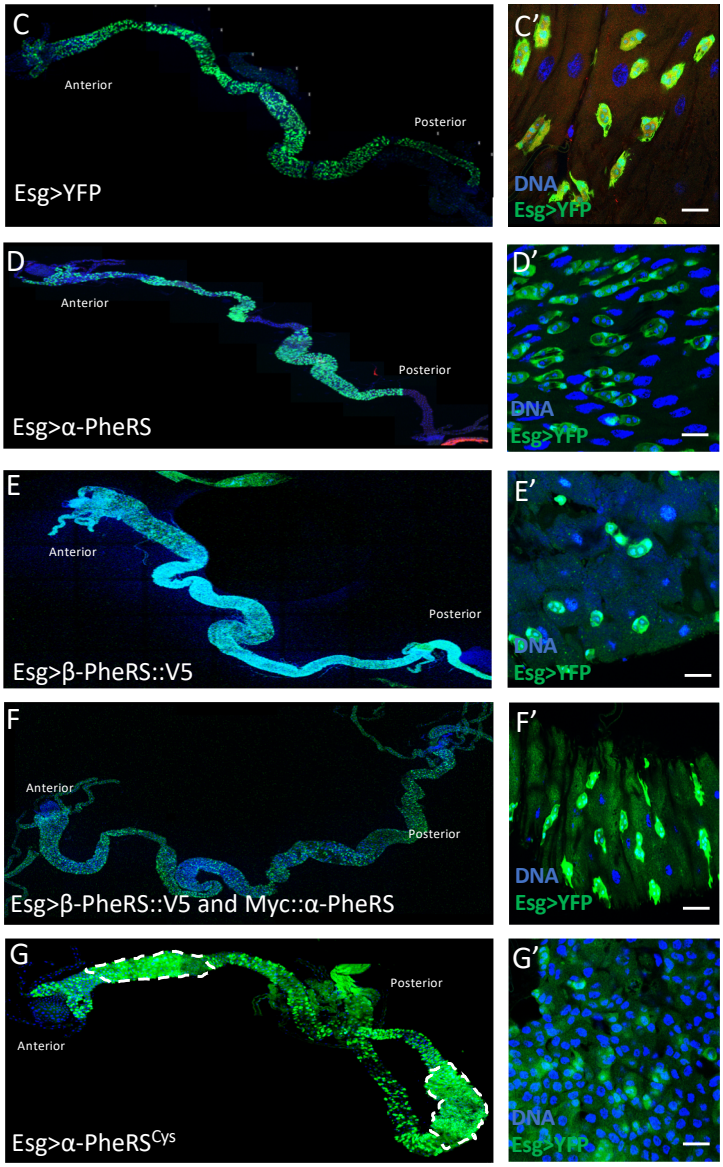

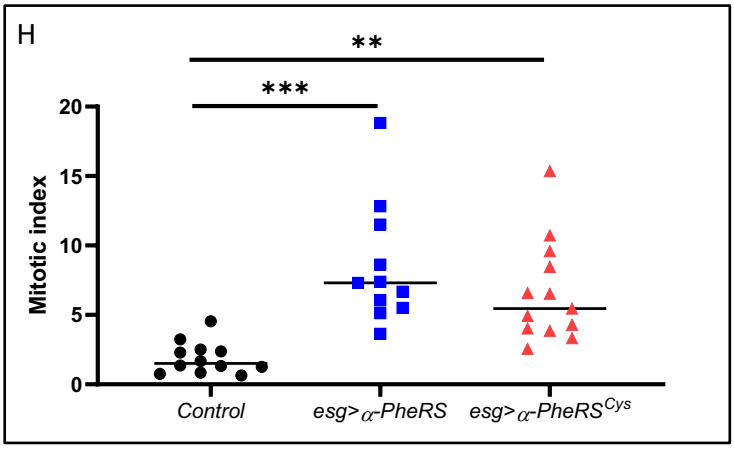

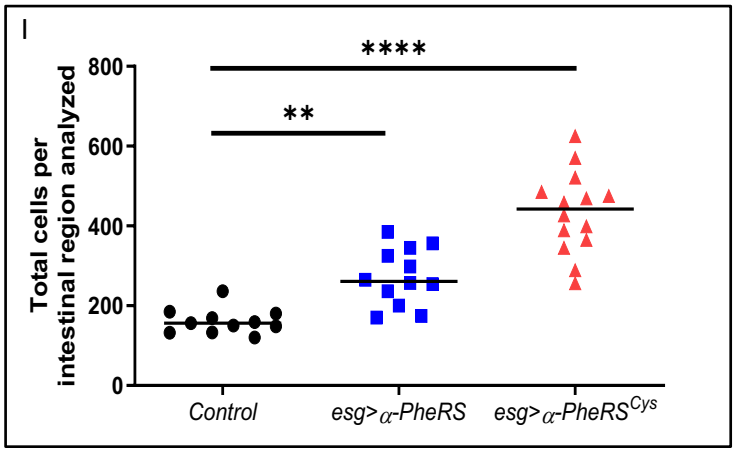

Adult midgut

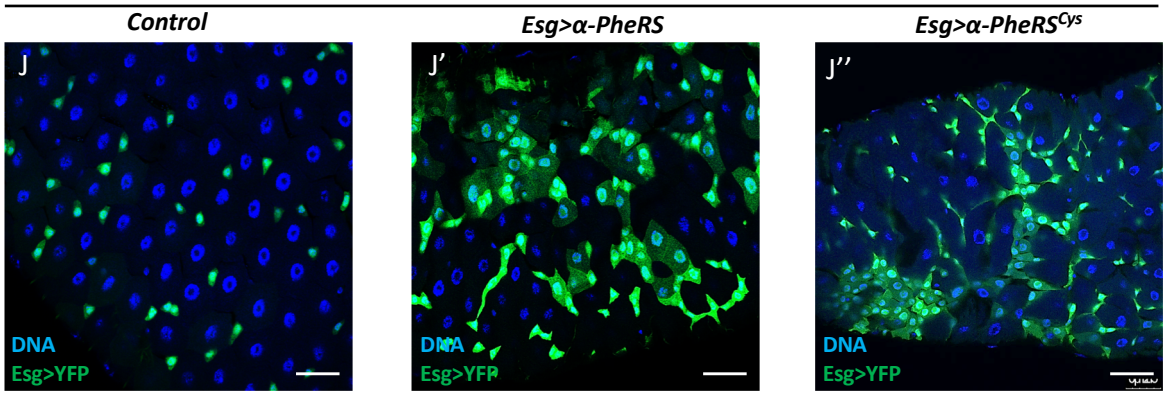

Figure 5

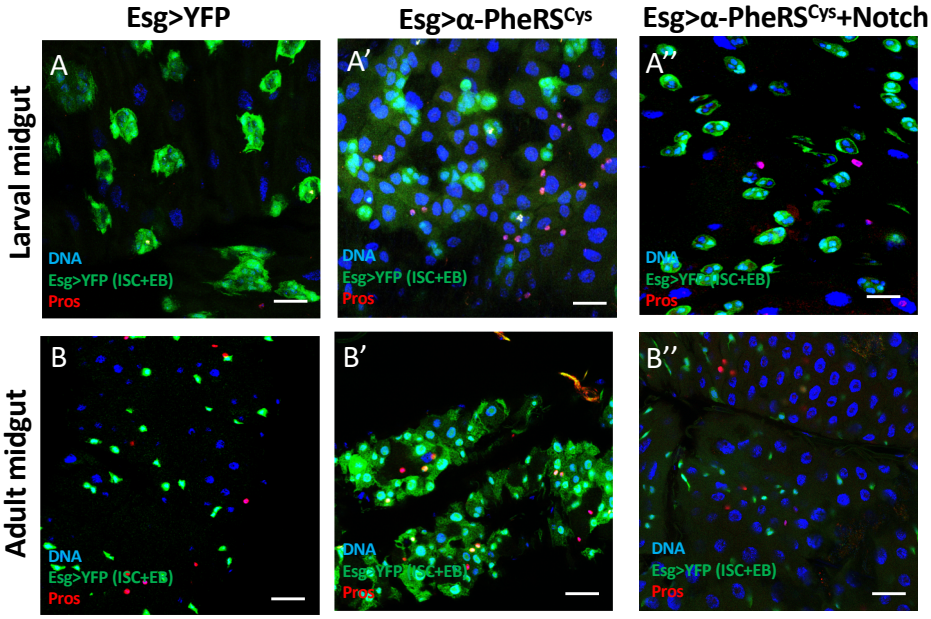
Esg>YFP
Esg>α-PheRS^Cys
Esg>α-PheRS^Cys+Notch
Larval midgut
Adult midgut
A
A'
A''
B
B'
B''
DNA
Esg>YFP (ISC+EB)
Pros

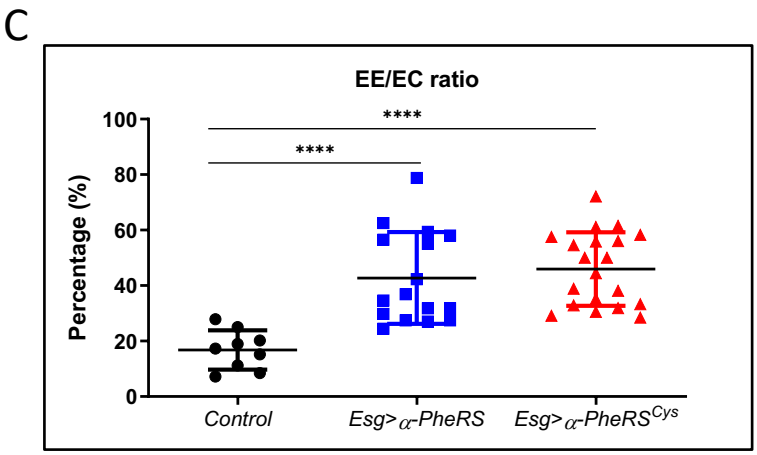
C
EE/EC ratio
Percentage (%)
100
80
60
40
20
0
****
****
Control
Esg>α-PheRS
Esg>α-PheRS^Cys

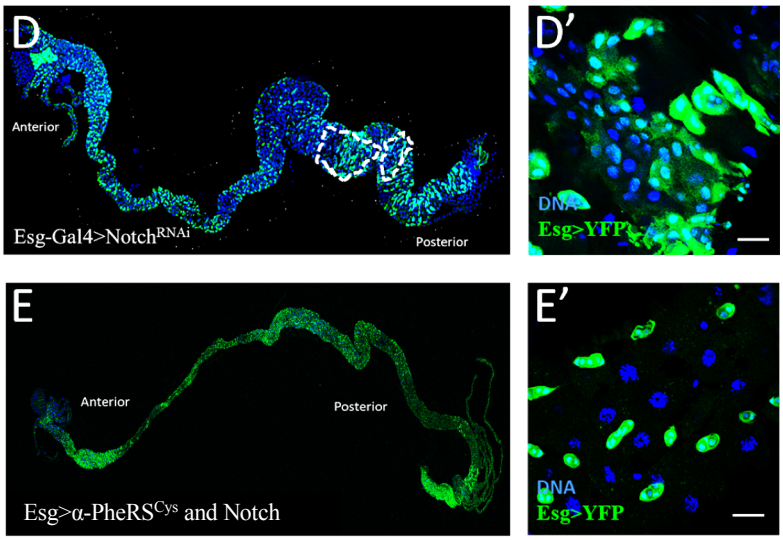
D
Anterior
Posterior
Esg-Gal4>Notch^RNAi
D'
DNA
Esg>YFP
E
Anterior
Posterior
Esg>α-PheRS^Cys and Notch
E'
DNA
Esg>YFP

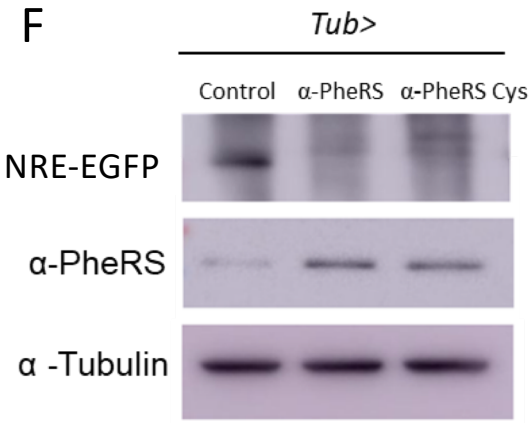
F
Tub>
Control
α-PheRS
α-PheRS Cys
NRE-EGFP
α-PheRS
α -Tubulin

Figure 6

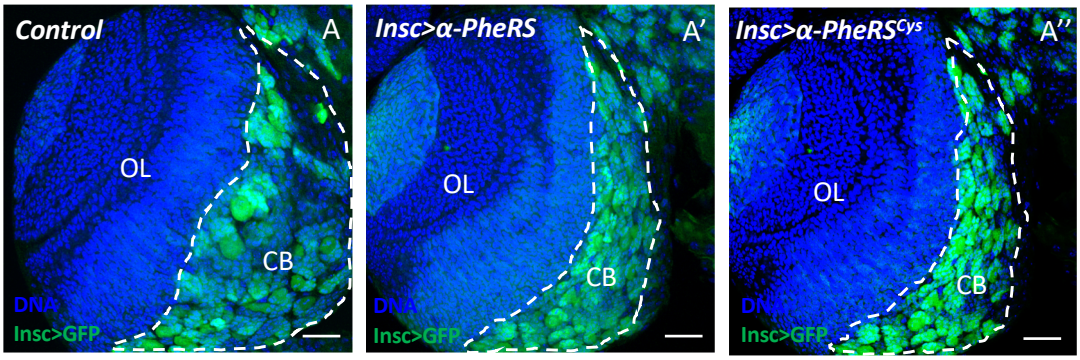
Control
A
OL
CB
DNA
Insc>GFP
Insc>α-PheRS
A'
OL
CB
DNA
Insc>GFP
Insc>α-PheRSCys
A''
OL
CB
DNA
Insc>GFP

B

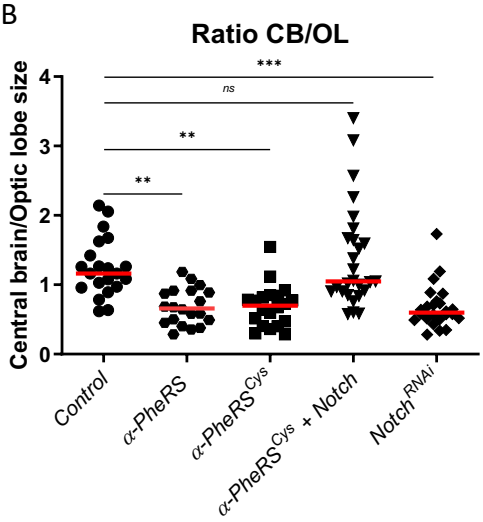
Ratio CB/OL
Central brain/Optic lobe size
0
1
2
3
4
***
ns
**
**
Control
α-PheRS
α-PheRSCys
α-PheRSCys + Notch
NotchRNAi

C

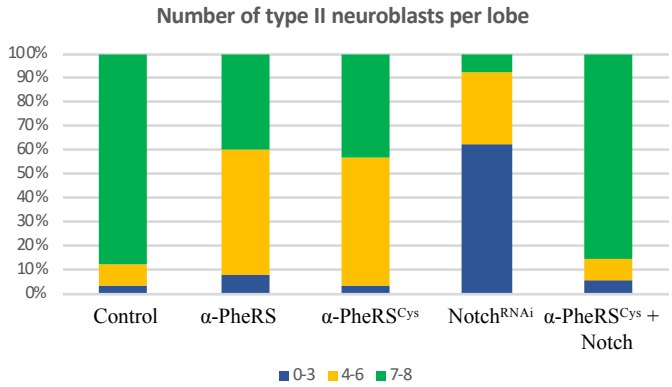
Number of type II neuroblasts per lobe
100%
90%
80%
70%
60%
50%
40%
30%
20%
10%
0%
Control
α-PheRS
α-PheRSCys
NotchRNAi
α-PheRSCys + Notch
0-3
4-6
7-8

Figure 7

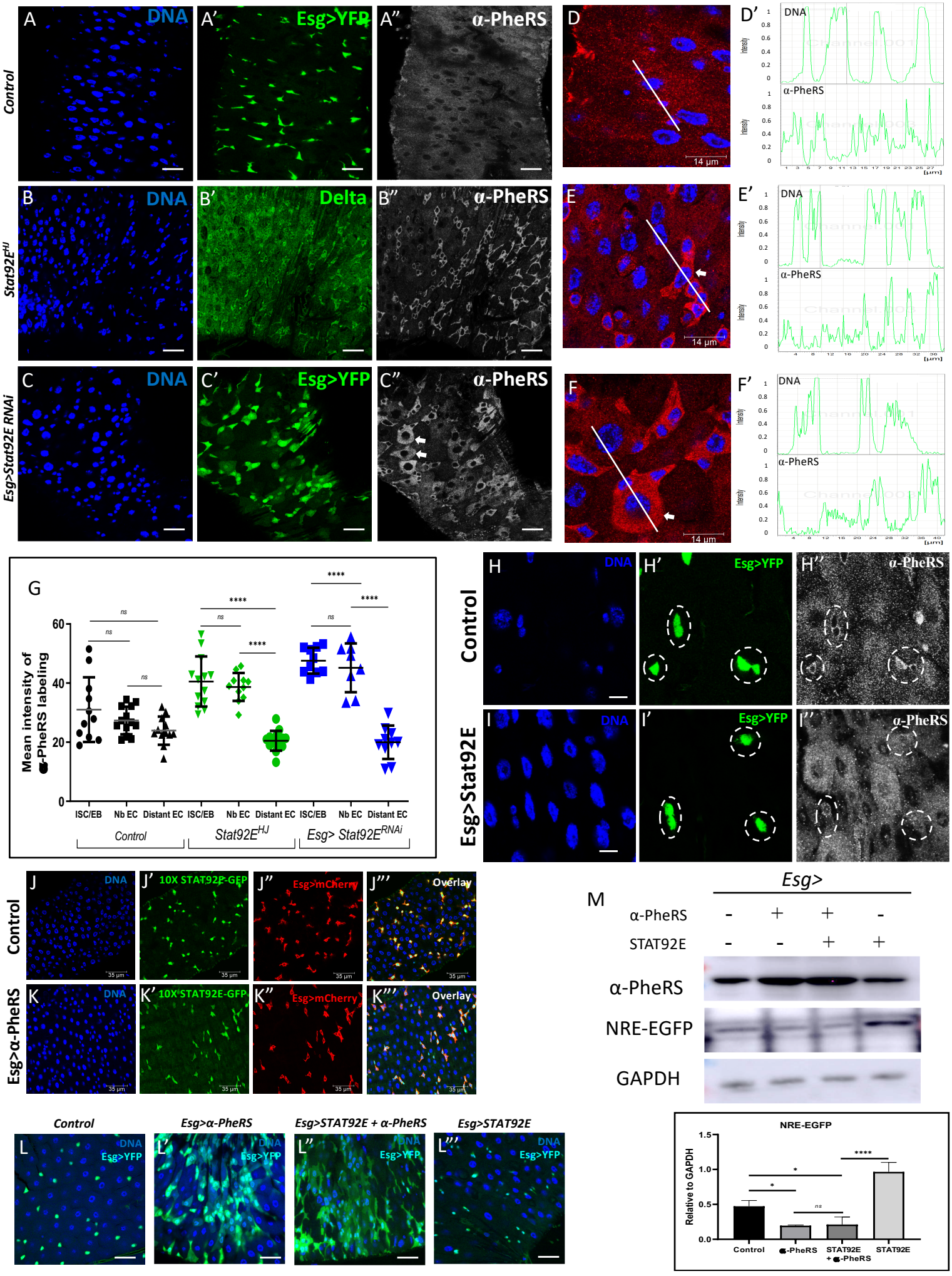
Control
Stat92E^HJ
Esg>Stat92E RNAi
A DNA
A' Esg>YFP
A'' α-PheRS
B DNA
B' Delta
B'' α-PheRS
C DNA
C' Esg>YFP
C'' α-PheRS
D
E
F
14 µm
D' DNA
α-PheRS
E' DNA
α-PheRS
F' DNA
α-PheRS
Intensity
G
Mean intensity of α-PheRS labeling
ISC/EB
Nb EC
Distant EC
Control
Stat92E^HJ
Esg> Stat92E^RNAi
ns
****
H DNA
H' Esg>YFP
H'' α-PheRS
I DNA
I' Esg>YFP
I'' α-PheRS
Control
Esg>Stat92E
J DNA
J' 10X STAT92E-GFP
J'' Esg>mCherry
J''' Overlay
K DNA
K' 10X STAT92E-GFP
K'' Esg>mCherry
K''' Overlay
Esg>α-PheRS
35 µm
M
Esg>
α-PheRS
STAT92E
NRE-EGFP
GAPDH
Control
Esg>α-PheRS
Esg>STAT92E + α-PheRS
Esg>STAT92E
L DNA Esg>YFP
L' DNA Esg>YFP
L'' DNA Esg>YFP
L''' DNA Esg>YFP
NRE-EGFP
Relative to GAPDH
Control
α-PheRS
STAT92E + α-PheRS
STAT92E

SUPPLEMENTARY DATA

Figure S1

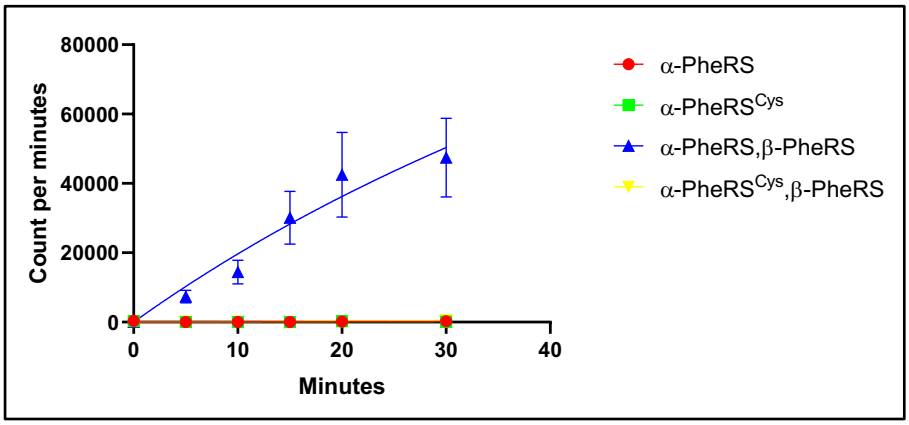

Figure S1:
The *α–PheRS*^{Cys} mutant does not support aminoacylation in vitro. The aminoacylation assay was performed with the mixture of the recombinant protein (α–PheRS or α–PheRS^{Cys} and β-PheRS) produced in E. coli. tRNA^{Phe} from yeast was aminoacylated with [^{3}H] phenylalanine. The [^{3}H] phenylalanine signal coupled with tRNA^{Phe} was counted by the radiometer. CPM= counts per minute.

Figure S2

Analyzing the size of dissociated larval wing disc cells by FACS revealed that the cells from the posterior compartment (GFP-positive compartment), where both PheRS subunits were overexpressed, were on average larger than the ones that overexpressed only GFP or only α-PheRS (A). In contrast, all control cells from the anterior (GFP-negative) compartment of these three lines were of similar, smaller size (A). Cell numbers, on the other hand, did not significantly change upon overexpression of both PheRS subunits (B). We conclude that in larval wing discs with their organ control mechanism, PheRS overexpression causes primarily an increase in cell size. On the other hand, single overexpression of α-PheRS increases the mitotic index of wing discs.

A

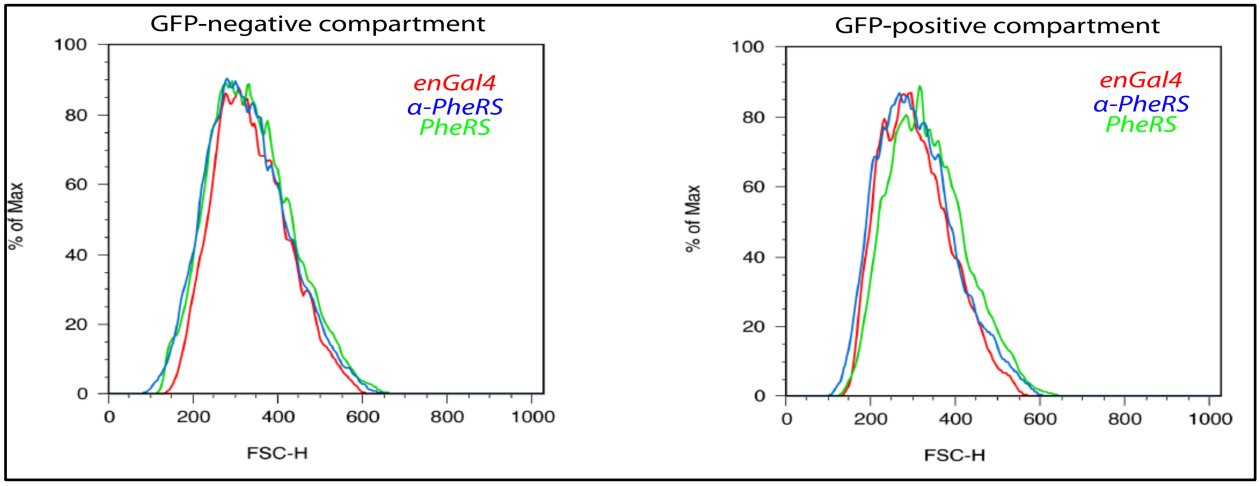

B

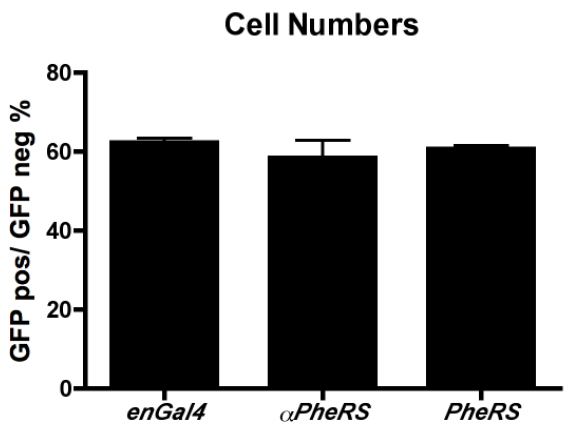

Figure S2: PheRS overexpression in wing discs increases cell size, but not cell numbers
(A) Cell size was determined by measuring the Forward Scatter (FSC) in the FACS analysis. Larvae were synchronized by using 2-hours egg lays. Late 3rd instar larvae were dissected and wing discs were dissociated. GFP was used to mark cell populations that express transgenes. The cells of the GFP-negative compartment showed similar cell size in the different lines (left panel). In the GFP positive compartment, where the transgenes were overexpressed, PheRS overexpression gave rise to bigger cells (right panel). This is the representation of the results of three independent experiments. (B) Cell numbers are not significantly altered by PheRS overexpression. The experimental set up was the same as in (A). Posterior cell numbers (P; GFP positive) were determined relative to the anterior (A; GFP negative) cell numbers (n=3).

Figure S3

Amino acid deprivation downregulates phosphorylation of dS6K in Kc cells, and subsequent stimulation with amino acids can restore this phosphorylation (Kim et al., 2008). The Rag complex is part of a nutrient sensor pathway, and its knockdown prevented the TORC1 complex from sensing the availability of amino acids (Kim et al., 2008; Sancak et al., 2008). In contrast, when *β-PheRS* was knocked down, amino acids were still able to induce phosphorylation of dS6K to similar levels as in the control. In this case, it did not matter whether all amino acids were added back (A) or only L-Phe (B). These results therefore suggest that PheRS does not serve as an amino acid sensor upstream of the TORC1 complex, although we cannot rule out that the knockdown was not sufficient to induce this effect.

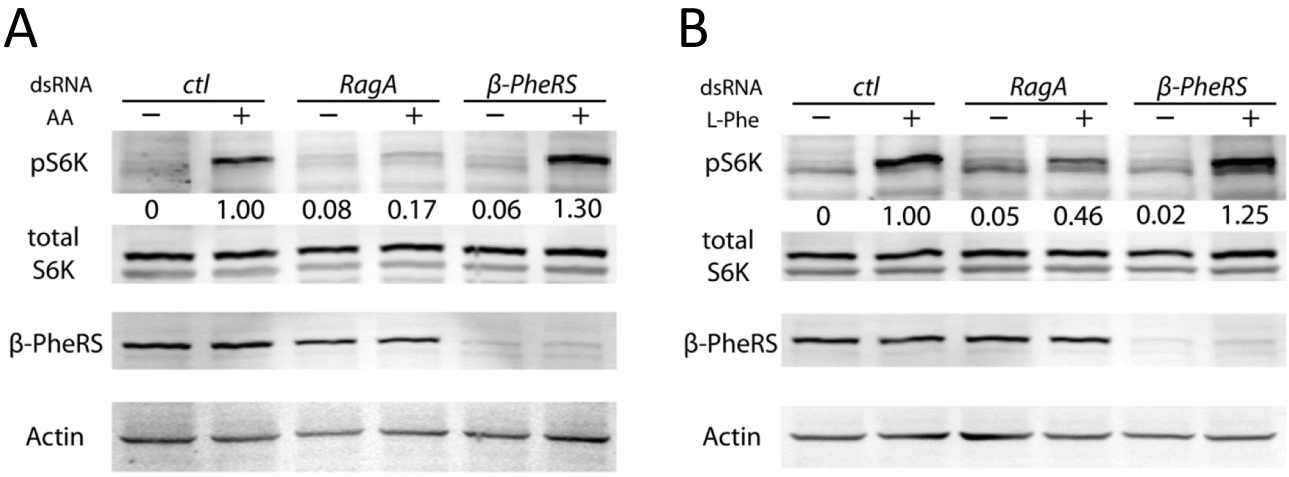

Figure S3: PheRS does not seem to serve as an amino acid sensor upstream of the TORC1 complex. (A) *β-PheRS* knockdown cannot block the TORC1 complex from sensing the availability of amino acids. Phospho-S6K was used as a readout of TORC1 signaling. Starvation (–) was performed by depriving cells from amino acids for 30 mins, and stimulation (+) was performed by adding back amino acids for 30 mins after starvation. Control is a mock RNAi, *Rag A* RNAi is known to block the sensing of amino acids. The level of phospho-S6K was quantified relative to the Actin level in the same extract. (B) *β-PheRS* knockdown cannot block the TORC1 complex from sensing the availability of L-Phe. The same experiment as in (A) was performed, but using L-Phe and L-Glu for stimulation. L-Glu was reported to be necessary for amino acid transport (Nicklin et al., 2009). Levels of phospho-S6K were quantified relative to the Actin levels in the same extract.

Figure S4

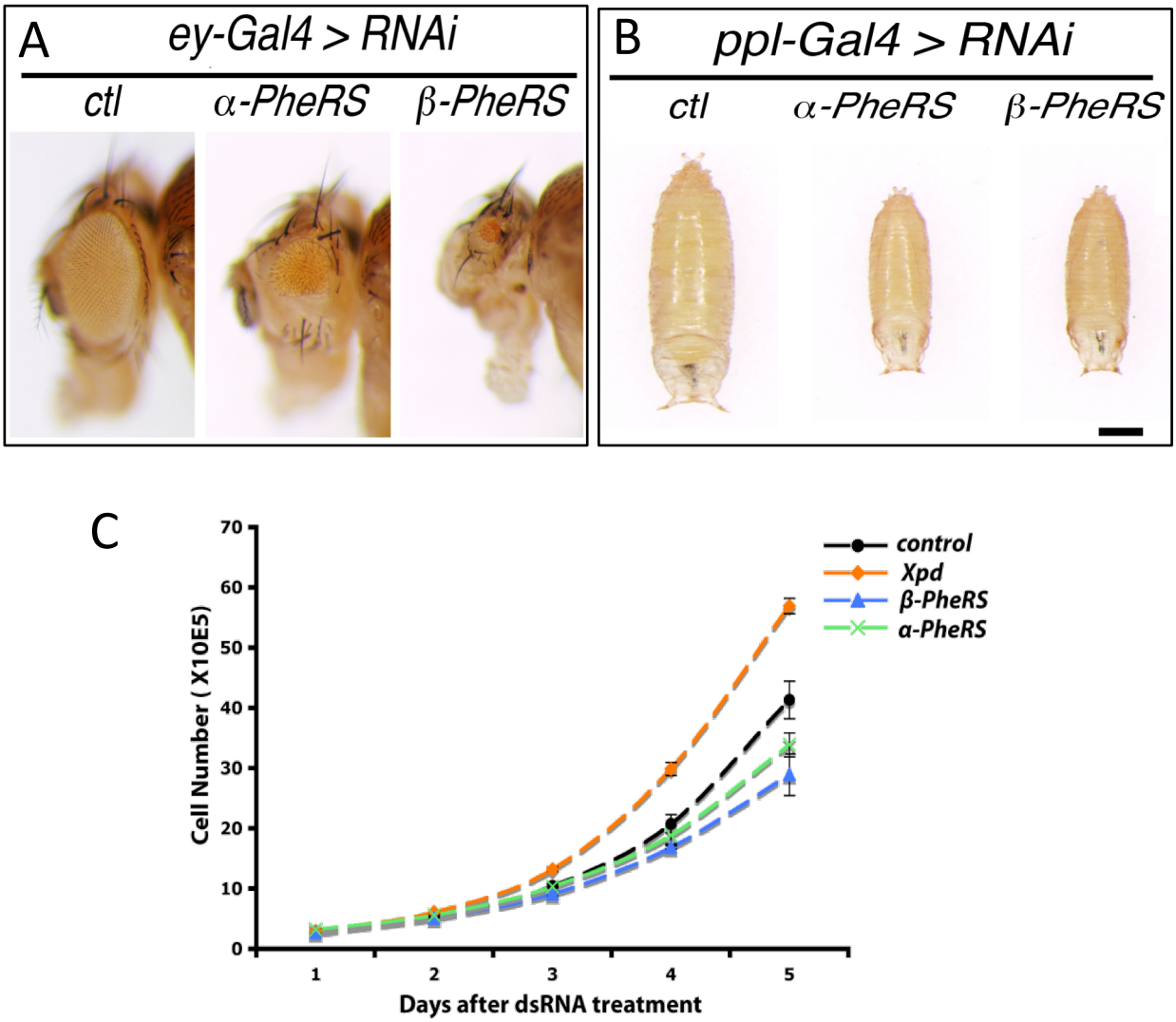

Figure S4: PheRS knockdown reduces cell proliferation and tissue size.
(A,B) RNAi knock down of *PheRS* subunits in the fly eyes (A) and fat bodies (B). *ey-Gal4* and *ppl-Gal4* were used to drive RNAi expression, respectively. The controls were GFP RNAi. RNAi knock down of either subunit reduced the eye size (A) and the size of the entire pupae, respectively. (C) Proliferation of Kc cells upon knockdown of the subunits. The control is *xpd* RNAi. RNAi knockdown was carried out by directly adding dsRNA to the medium, and cells were harvested at days 1, 2, 3, 4, and 5 after dsRNA treatment. Knockdown of either subunit reduces cell proliferation and downregulates levels of both subunits (Lu et al., 2014).

Figure S5

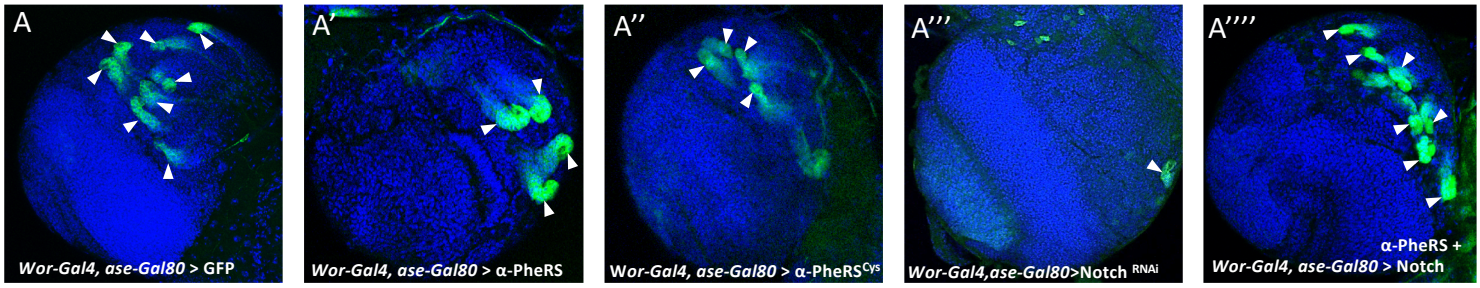

Figure S5: The overexpression of *α-PheRS* or *α-PheRS^{Cys}* in type II NBs reduced the number of type II NBs per central brain. *wor-Gal4,ase-Gal80,UAS-GFP* was used to overexpress proteins in type II NBs. Type II NBs were labelled by GFP expression and marked with white arrowheads.